



# Emissions relationships in western forest fire plumes – Part 1: Reducing the effect of mixing errors on emission factors

Robert B. Chatfield<sup>1</sup>, Meinrat O. Andreae<sup>2,3</sup>, ARCTAS Science Team<sup>+</sup>, and SEAC4RS Science Team<sup>+</sup>

<sup>1</sup>NASA Ames Research Center, Moffett Field, CA 94035, USA

<sup>2</sup>Max Planck Institute for Chemistry, P.O. Box 3060, 55020 Mainz, Germany

<sup>3</sup>Scripps Institution of Oceanography, UCSD, La Jolla, CA 92093, USA

<sup>+</sup>A full list of authors appears at the end of the paper.

**Correspondence:** Meinrat O. Andreae (m.andreae@mpic.de) and Robert B. Chatfield (chatfield@alumni.rice.edu)

Received: 10 June 2019 – Discussion started: 15 August 2019

Revised: 26 August 2020 – Accepted: 29 August 2020 – Published: 23 December 2020

**Abstract.** Studies of emission factors from biomass burning using aircraft data complement the results of lab studies and extend them to conditions of immense hot conflagrations. A new theoretical development of plume theory for multiple tracers is developed after examining aircraft samples. We illustrate and discuss emissions relationships for 422 individual samples from many forest fire plumes in the Western USA. Samples are from two NASA investigations: ARCTAS (Arctic Research of the Composition of the Troposphere from Aircraft and Satellites) and SEAC4RS (Studies of Emissions and Atmospheric Composition, Clouds and Climate Coupling by Regional Surveys). This work provides sample-by-sample enhancement ratios (EnRs) for 23 gases and particulate properties. Many EnRs provide candidates for emission ratios (ERs, corresponding to the EnR at the source) when the origin and degree of transformation is understood. From these, emission factors (EFs) can be estimated, provided the fuel dry mass consumed is known or can be estimated using the carbon mass budget approach. This analysis requires understanding the interplay of mixing of the plume with surrounding air. Some initial examples emphasize that measured  $C_{\text{tot}} = \text{CO}_2 + \text{CO}$  in a fire plume does not necessarily describe the emissions of the total carbon liberated in the flames,  $C_{\text{burn}}$ . Rather, it represents  $C_{\text{tot}} = C_{\text{burn}} + C_{\text{bkgd}}$ , which includes possibly varying background concentrations for entrained air. Consequently, we present a simple theoretical description for plume entrainment for multiple tracers from the flame tops to hundreds of kilometers downwind and illustrate some intrinsic linear behaviors. The analysis suggests a mixed-effects regression emission technique

(MERET), which can eliminate occasional strong biases associated with the commonly used normalized excess mixing ratio (NEMR) method. MERET splits  $C_{\text{tot}}$  to reveal  $C_{\text{burn}}$  by exploiting the fact that  $C_{\text{burn}}$  and all tracers respond linearly to dilution, while each tracer has consistent EnR behavior (slope of tracer concentration with respect to  $C_{\text{burn}}$ ). The two effects are separable. Two or three or preferably more emission indicators are required as a minimum; here we used eight. In summary, MERET allows a fine spatial resolution (EnRs for individual observations) and comparison of similar plumes that are distant in time and space. Alkene ratios provide us with an approximate photochemical timescale. This allows discrimination and definition, by fire situation, of ERs, allowing us to estimate emission factors.

## 1 Introduction

### 1.1 Importance and previous work

Biomass burning has a large influence on the atmospheric burden of ozone and aerosols and consequently also affects climate (Crutzen et al., 1979; Crutzen and Andreae, 1990; Jaffe and Wigder, 2012; Andreae, 2019; Galanter et al., 2000). Biomass-burning emission factors that are useful for driving photochemical models are most often estimated by one of two sampling techniques (Crutzen et al., 1979; Crutzen and Andreae, 1990; Koppmann et al., 1997; Galanter et al., 2000; Jaffe and Wigder, 2012; Akagi et al., 2013; Andreae, 2019). In the first approach, measurements

on the ground close to an open fire or on laboratory fires that are controlled to approximate natural conditions can provide the most detailed information on sources. The burning conditions can be readily assessed and fit into parameterizations of the emissions process, provided the correct mix of burn types typical of large fires can be estimated. It can, however, be difficult to mimic and safely sample truly intense flaming conflagrations. In the second approach, measurements made from aircraft provide a much wider sample of different fires and emissions from different regions of a single fire. However, the estimates can be difficult to classify as simply “flaming” or “smoldering” or even as defined mixtures of just two types. Adjoining areas with fires in various stages of combustion can merge into the same plume or remain relatively distinct. These questions of classifications related to the originating fires will be addressed statistically in a succeeding paper (Chatfield and Andreae, 2020).

This work presents a rationale for more mathematically thorough attention in the estimation of emissions relationships and emission factors in contrasting case studies and uses such studies to develop an entraining-plume theory for emissions relationships. Illustrations show that this theory gives intuitively reasonable results in some more complex situations. This theory suggests a statistical regression technique; a second methodology section then gives details of implementation given the complexities of atmospheric sampling. The result, a key “equivalent-background” estimate, is then applied to quantify the atmospheric signal of fuel burned, approximately the sum  $\text{CO}_2 + \text{CO}$ ; this allows quantification of emission factors.

Let us introduce our view of enhancement ratios, emission ratios, and emission factors. Under appropriately defined circumstances, the amount of fuel carbon burned that is liberated to the atmosphere is the sum of carbon added to the ambient air in the form of all fire-originated gases and particles as a result of combustion: in deriving emission factors, i.e., how much of a species is emitted per kilogram of biomass burned, it is usual to obtain the amount of carbon burned by taking the difference in the sum of excess mixing ratios,  $\text{CO}_2 + \text{CO} + \text{other carbon-containing emissions}$ , including aerosol particles. To an accuracy of within 1.5 % (totals from the datasets we analyzed) to 3 % (Andreae and Merlet, 2001), carbon burned or  $C_{\text{burn}}$  is approximated by the excess ( $\text{CO}_2 + \text{CO}$ ), as measured above a background concentration,  $C_{\text{bkgd}}$  (Andreae et al., 1988):

$$C_{\text{Burn}} = \Delta C_{\text{Tot}} = \Delta \text{CO}_2 + \Delta \text{CO} + \Delta \text{CH}_4 \\ + \Delta(\text{particulate carbon}) + \Delta(\text{O})\text{VOCs},$$

approximated here as

$$C_{\text{Burn}} = \Delta C_{\text{Tot}} \approx \Delta \text{CO}_2 + \Delta \text{CO},$$

and for graphics and theory,

$$C_{\text{Tot}} = x, \quad C_{\text{Burn}} = x - x^0 = C_{\text{Tot}} - C_{\text{Bkgd}}, \quad (1)$$

where  $\Delta$  refers to the enhancement relative to preburn air and (O)VOCs refer to the carbon content of volatile organic species, possibly oxygenated (O). In measurement situations where frequent, accurate measurements of  $\text{CH}_4$  and particulate C are also available, their inclusion could add < 1 % precision to the estimates. Analysis proceeds similarly including these terms. This work uses some algebra and graphics, so we introduce  $x = C_{\text{Tot}}$  and  $x^0 C_{\text{Bkgd}}$ .

An enhancement ratio (EnR) for a species or property  $j$  with mixing ratio  $y_j$  is then  $\text{EnR}_j = \Delta y_j / \Delta C_{\text{Burn}}$ . We will use this term enhancement ratio, EnR, in this paper. When EnRs are sampled prior to substantial atmospheric transformation (e.g., chemistry or particulate processes), they describe emission ratios (ERs). More on the relationships of EnRs, ERs, and emission factors (EFs) is found in the Supplement, “Note on EnRs and ERs”. ER estimation constitutes the analysis of atmospheric samples that contribute to EFs. Emission factors are defined relative to the amount of fuel burned and are derived from emission ratios by accounting for the concentration of carbon in the biomass burned and adjustment of units (Andreae and Merlet, 2001). Separate methods of land analysis are employed. EFs can be derived from ERs by

$$\text{EF}_j = \text{ER}_j \times \frac{\text{MW}_j}{\text{MW}_c} \times C_{\text{BM}}, \quad (2)$$

where  $\text{ER}_j$  is the emission ratio of species  $j$ ;  $\text{MW}_j$  and  $\text{MW}_c$  are the molecular weight of species  $j$  and the atomic weight of carbon, respectively; and  $C_{\text{BM}}$  is the carbon content of the dry biomass. We focus on improving methods of finding EnRs and ERs, which enable EF estimation.

One part of EF estimation concerns the amount of fuel consumed in fires, its carbon content, and the fraction liberated to the atmosphere (i.e., excluding char remaining on the ground); here we will focus on the other part of the question, which concerns the relationship of emitted compounds to the C liberated to the atmosphere. Many of the EnRs we calculate appear to be good candidates for EF estimates. One remaining task, making specific links of particular EFs to appropriate fire conditions to which they apply, requires individualized trajectories and fuel characterizations. This task, relating atmospheric signals of fuel burned to the details of the surface burning of carbon, is beyond reasonable treatment in this publication, which focuses on improving the understanding of airborne samples. It seems likely to us that uncertainties in the relation of area and fuel burned contribute more error to emissions estimates than those contributions of minor C-containing species in the plume that were described above.

There are other uses for EnRs that arise in understanding fire plumes, which revolve around the evolution of relatively fresh smoke plumes, e.g., the enhancement of ozone, peroxy acetyl nitrate, or other bound (not NO or  $\text{NO}_2$ ) nitrogen species (Alvarado and Prinn, 2009; Akagi et al., 2012; Baylon et al., 2015; Alvarado et al., 2009, 2010; Jaffe and

Widger, 2012). These also should have a direct relation to the fuel carbon burned and other properties such as burning conditions, fuel moisture, and fuel  $N$  content.

A complication arises from the fact that preburn or non-burned air may have various compositions, especially when we consider various sources for low-level inflow air and especially air that is entrained in the smoke plume by the time of sampling. This is an important topic, which has been discussed in detail by Guyon et al. (2005) and Yokelson et al. (2013) and which we will focus on below.

Two special intensive-sampling missions utilizing NASA's fully instrumented DC-8 aircraft allowed us to investigate forest-burning emissions. In June 2008, the aircraft sampled a variety of fire plumes around California (Jacob et al., 2010; Singh et al., 2010, 2012; Hornbrook et al., 2011) during the California ARCTAS (Arctic Research of the Composition of the Troposphere from Aircraft and Satellites) intensive period. In a later part of the campaign, the DC-8 sampled plumes in Northern Canada (Simpson et al., 2011); we excluded these plumes as representing different, more boreal, forest burn conditions. In 2013, the DC-8 made several samplings of forest fires in California and the Rocky Mountain West during SEAC4RS (Studies of Emissions and Atmospheric Composition, Clouds and Climate Coupling by Regional Surveys; Toon et al., 2016). We analyzed all of these fire plumes but excluded samples east of  $102^\circ$  W, which were mostly from agricultural fires. Our aim was to understand a variety of plumes but limit variation to a single general category (temperate forest fires) as used for three-dimensional simulation models and geographical summaries.

Flight tracks for the period and locations of major fires during these periods are shown in Fig. 1. Analysis of the vertical variation in fire tracers suggested that plumes below 5 km a.s.l. included recent and informative fires in our study. We saw no unequivocal variation in composition with height, possibly due to limitations on aircraft maneuvers low and near the fires. Consequently, the aircraft samples likely cannot adequately represent ground-hugging smoke flows.

## 1.2 Development of EF estimation to date

EnRs and EFs for biomass-burning plumes have largely been based on measurements of the  $\text{CO}_2$  or CO concentrations in the plumes. Typical analyses begin with measurements of  $C_{\text{tot}}$  and the concentrations of several tracers we may call  $y_j$ :  $j = 1, \dots, N_{\text{Tracers}}$ . Multiple instances,  $i = 1, \dots, N_{\text{Instances}}$ , are observed, e.g., every few seconds or few minutes within a plume. An affine dependence (linear polynomial relationship including an intercept) is observed between each of the tracers and  $C_{\text{tot}}$  with a  $y$  intercept that depends most significantly on the local out-of-plume background values of  $\text{CO}_2$ , CO, and each tracer individually.

$$C_{\text{tot}} = C_{\text{bkgd}} + C_{\text{burn}} \quad (3)$$

The following analysis suggests several complexities that must be addressed in order to understand these affine relationships. Several aspects of slopes, intercepts, and deviations from linearity of the relationship of tracer  $y_j$  to  $C_{\text{tot}}$  plots must be examined, and so we transition to graphic terminology with  $x$  representing  $C_{\text{tot}}$ . Later we will describe measurements of  $C_{\text{tot}}$  and tracers  $j$  at a given instance  $i$ ,  $x_i$  and  $y_{ij}$ . For a simple plume within a homogeneous mixed layer characterized by an  $x$  concentration  $x^0$  and  $y$  concentration  $y^E$ , we write

$$x = x^0 + (x - x^0) \quad (4)$$

and

$$(y_j - y_j^E) = a_j (x - x^0), \quad (5)$$

with an enhancement ratio,  $a_j$ , that can yield EnRs directly. Early estimations (e.g., Greenberg et al., 1984; Andreae et al., 1988) used plots and regressions against  $\text{CO}_2$  to estimate EnRs and EFs. These earliest techniques assumed fire was the main origin of  $\text{CO}_2$ . Very early it was recognized that other effects, e.g., variation in photosynthesis, respiration, and mixing, required a more sophisticated approach (e.g., Guyon et al., 2005). Alternatively (e.g., Andreae et al., 1988; Hobbs et al., 2003; Lefer et al., 1994), EnRs were derived with respect to CO. Symbolically,

$$\begin{aligned} \text{EnR estimate} &= \text{Estimate}\left(\frac{\delta y_j}{\delta \text{CO}}\right) \cdot \text{Estimate}\left(\frac{\delta \text{CO}}{\delta \text{CO}_2 + \delta \text{CO}}\right) \\ &= (\text{Regression slope of } y_j \text{ on CO}) \\ &\quad \cdot (\text{Regression slope of CO on } (\text{CO}_2 + \text{CO})). \end{aligned}$$

Here we use the symbol  $\delta$  to indicate that these differences are evaluated from sequential samples or a regression of such a sequence. The second factor is based on the modified combustion efficiency (MCE),

$$\begin{aligned} \text{MCE} &= \delta \text{CO}_2 / (\delta \text{CO}_2 + \delta \text{CO}) \\ &= 1 - \delta \text{CO} / (\delta \text{CO}_2 + \delta \text{CO}) \\ &= 1 - \text{EnR}_{\text{CO}}, \end{aligned} \quad (6)$$

with an attempt to estimate the domain of points for which a constant MCE could be assumed. The form of the difference symbol is written so as to emphasize that the differences are typically taken from a contiguously sampled time series of observations.

The method has become known as the normalized excess mixing ratio (NEMR) method (Akagi et al., 2011). Yokelson et al. (2013) described the care required to make sure that the MCE was well defined; otherwise, severe difficulties ensue. They describe a situation in which  $x^0$  and  $y_{\text{CO}}^E$  in a diluting plume took on two distinct values, a mixed-layer value and a free-troposphere value, during plume rise and transport. More than two values may be relevant, emphasizing their call for a more thorough sampling of prefire air and

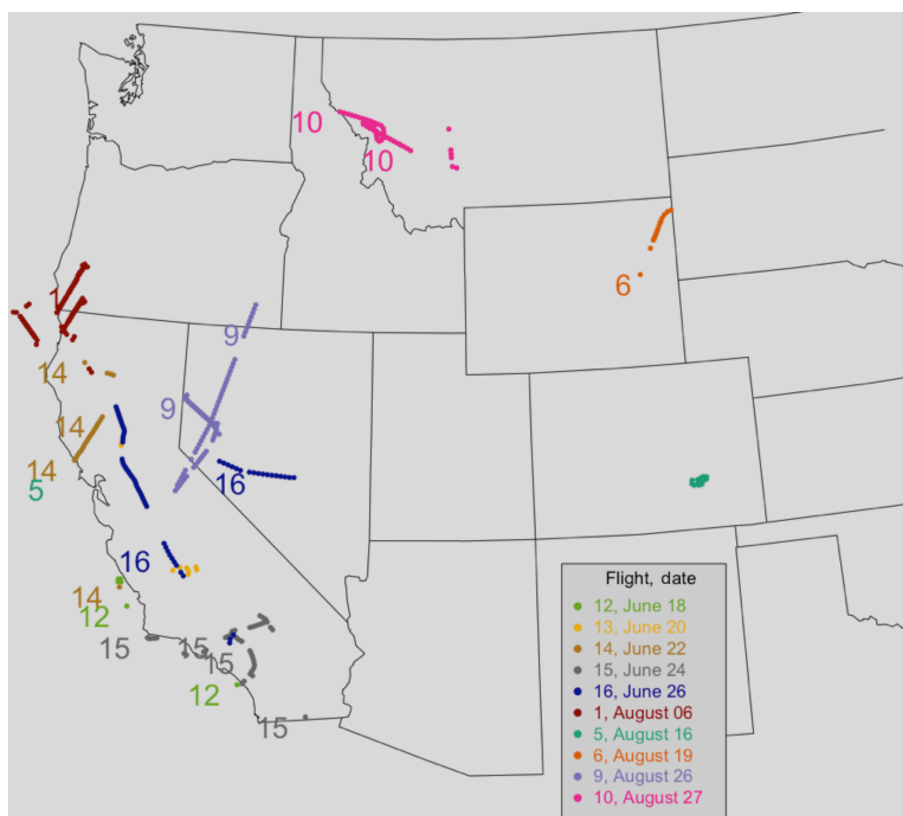


**Figure 1.** ARCTAS and SEAC4RS flights analyzed in this work. Each flight is identified by the flight number of that series. Flights 5 and 6 were in the Western USA but not included.

its dilution environment. We describe below new methods to resolve many of the difficulties with  $x^0$  and to indicate unwanted effects of  $y_{\text{CO}}^{\text{E}}$  variability. These methods could provide EnRs for many species with reasonable precision under more conditions.

This need for caution was very evident in the ARCTAS and SEAC4RS observational situations. Some Western USA data we analyzed showed variations in background  $C_{\text{tot}} = \text{CO}_2 + \text{CO}$  (away from direct recent effects of respiration and photosynthesis) of 15 ppm (interquartile range of 4 ppm), while other Western USA regions showed variations of  $\sim 8$  ppm (according to the analyses in this paper that we present later in Fig. 4). The contributions from fires were often comparable to this variation,  $\sim 2\text{--}40$  ppm, mean  $\sim 6$  ppm. Air flowed from the west into forest fires at low altitudes or later diluted the smoke plume at intermediate levels. We could expect background air with a variety of histories of influence by photosynthesis (lower resultant  $\text{CO}_2$ ) or respiration (higher  $\text{CO}_2$ ), or we could expect urban-influenced air (higher  $\text{CO}_2$ ). Low-level inflow air could have been mostly affected by local forests, farming, etc. Some of the most problematic situations tend to be associated with plumes sampled early in the day, when air from a nocturnal boundary layer – strongly enriched with respiration  $\text{CO}_2$  – is mixed into the smoke plumes (Guyon et al., 2005). There could also

have been substantial variations in  $C_{\text{tot}}$  due to intercontinental transport, the composition reflecting long-term previous modification due to these same processes and to latitudinal gradients. Yates et al. (2011) reported and more fully referenced atmospheric sampling of western air showing variations in  $\text{CO}_2$  and also in  $\text{CH}_4$  and  $\text{O}_3$ . On the east side of the Pacific anticyclone, the common pattern was for descent and horizontal-shearing displacements, producing substantial  $C_{\text{tot}}$  variations in both horizontal and vertical directions (Barry and Chorley, 1998).

Previous analyses have been made for the ARCTAS data, by Simpson et al. (2011) for the large Canadian fires sampled and by Hornbuck et al. (2011) for all fires. The Hornbuck article usefully complements this paper by describing features and origins of the plumes sampled. Both groups described novel methods but followed the traditional CO emissions ratio or NEMR methodology (Andreae et al., 1988; Hobbs et al., 2003; Akagi et al., 2011). Pfister et al. (2011) considered the emissions and transport of CO in the California ARCTAS samples. Analyses of the SEAC4RS fires have also been reported (Liu, 2017).

The following sections provide motivation for and understanding of an alternate approach to the description of EnRs and EFs, the mixed-effects regression emission technique, MERET; in some cases, MERET and the NEMR method

may form complementary supporting views of plume emissions. Whereas the NEMR approach depends on multiple measurements in the same plume in an understood environment, MERET is typically applicable to individual measurements of similar EnR-determining fire conditions across many different plumes. It instead requires several informative fire tracer species, not simply  $\text{CO}_2$  or  $\text{CO}$ , be measured simultaneously, as well as the tracer whose EnR is desired. It can also be used for good candidate EFs when the environmental history of the plume is not well characterized. It is applicable to any plumes encountered, without need for extensive measurement of that plume history.

MERET attempts to use the simultaneous variability, sample by sample, of a large set of fire tracer compounds and aerosol descriptors to find a single quantification,  $C_{\text{burn}}$ , of fire emissions, which it splits from  $C_{\text{bkgd}}$  such that the sum is  $C_{\text{tot}}$ . To do so, it must also ascribe a set of EnRs to the fire tracers and recognize that these EnRs may vary from sample to sample in a limited way. The interplay of these estimates contributing to  $C_{\text{burn}}$  and EnRs for each observation appears daunting. Section 3 will graphically illustrate how strongly effects beyond fire emissions describe variations in  $C_{\text{tot}}$  and also how similar and informative various tracers are as graphed against  $C_{\text{tot}}$ . Section 4 will describe a theory of multiple fire emissions co-emitted from a fire based on familiar plume concepts and give examples. The examples show the linearity of the theory that such simple approaches with a limited number of parameter estimates yield a reasonable approximation to more complex behavior. Sections 5 and 6 describe a mixed-effects regression algorithm based on plume theory. Section 7 provides a limited number of EnR estimates and describes graphically how flight segments describing similar emissions conditions can be identified.

## 2 Methodology – defining an indicator dataset

An initial task is the identification of tracers that are informative about burning and sampling rates. The technique we describe requires the measurement of  $C_{\text{tot}} \approx \text{CO}_2 + \text{CO}$  and several concentrations of emitted species or similar, extensive, properties of emissions (e.g., dried-airstream scattering coefficients,  $b_{\text{scat}}$ ), which we will call *emission indicator species* or tracers. A set of indicator species was chosen for this publication to enable deriving relevant EnRs and to support our initial classification (e.g., flaming, smoldering, high- $N$  fuel). It is important to have as many differently behaving emission indicator species as possible, as different indicators may respond differently to different fuels and fire intensities (“fire chemistries”), and such variations are usually not known before analysis. We favored indicator species with rapid sampling rates, so as to define  $C_{\text{burn}}$  for the maximum number of instances, but certain variables like  $\text{CO}$ ,  $\text{CH}_4$ , and  $b_{\text{scat}}$  had special claims, as they can be maximally expressed in important types of fires. For our samples, methane and methanol

showed significant idiosyncracies. Their cumulative probability distribution differed from all other tracers, with prominently very high concentrations and much higher positive skewness. We surmise that this behavior resulted from other prominent sources, e.g. cattle raising, or that very long distance transport and long lifetimes caused very great nonfire sources, like  $\text{CO}_2$ . It was convenient to use these same frequently measured indicator variables to define  $C_{\text{burn}}$  and also for classification of fire chemistries. For classification, we added intensive variables, essentially ratios that should be physically independent of  $C_{\text{burn}}$ .

The emission indicator species that satisfied these requirements for both missions are shown in Table 1, along with references to the measurement techniques and observers. Only extensive quantities (proportional to  $C_{\text{burn}}$ ) are used in this paper.  $\text{CO}_2$  was measured by Stephanie Vay (ARCTAS) and Andreas Beyersdorff (SEAC4RS) using the AVOCET instrument (Vay et al., 2011). In examining EnRs for various species, we also use the organic aerosol (OA) measurements (Wagner et al., 2015). ARCTAS and SEAC4RS data sites give full information, as instrumentation characteristics naturally vary somewhat between missions (<https://www-air.larc.nasa.gov/cgi-bin/ArcView/arctas>, last access: 12 August 2020; <https://www-air.larc.nasa.gov/cgi-bin/ArcView/seac4rs?DC8=1>, last access: 12 August 2020).

Our techniques use algorithms that currently allow few missing observations among the variables. The sampling rates for emission indicators measured by PTRMS (proton-transfer ionization mass spectrometry) differed between the two aircraft missions. The SEAC4RS mission acquired suitably complete PTRMS-derived datasets at a  $1 \text{ min}^{-1}$  rate, and this defined the data interval used for both datasets. Additionally, in SEAC4RS  $\text{CO}$  was measured only by (less frequent) can samples for the first flights prior to the Rim Fire of 26 August 2013, and  $\text{CH}_4$  was sampled only by cans for all flights. These are important species:  $\text{CO}$  is the most commonly used tracer for fire plumes because of its favorable plume-to-background concentration ratio and readily available measurement instrumentation. It is also used to define the MCE in much of the biomass-burning literature (Yokelson et al., 1996; Jaffe and Widger, 2011). Consequently, SEAC4RS imposed additional difficulties and processing. However, we judged it important to include SEAC4RS in a combined analysis to broaden the fire chemistries analyzed, as the Rim Fire was exceptionally large, hot, and well sampled.

The selection of fire plumes required some care. While  $\text{CH}_3\text{CN}$  is a highly specific tracer of fires (Singh et al., 2012), detailed analysis suggests that it is not the best quantitative tracer. (Further analysis suggested that  $\text{CH}_3\text{CN}$  has variable EFs, so it signals fires well but does not quantify  $C_{\text{burn}}$  adequately.) Plumes were characterized by levels of  $\text{CH}_3\text{CN}$  above 0.225 ppb, over 4 times the assumed background of 0.054 ppb. Since some plumes are known to be quite low in gas-phase emissions, a few samples with lower  $\text{CH}_3\text{CN}$  mix-

**Table 1.** Indicator variables.

Concentration or property	Abbreviation	Technique	Group	Reference
Extensive quantities	Proportional to total burned material, as measured by $C_{\text{burn}}$			
Toluene	$C_6H_5CH_3$	PTRMS	Wisthaler	Wisthaler et al. (2014)
Benzene	$C_6H_6$	PTRMS	Wisthaler	Wisthaler et al. (2014)
Formaldehyde	HCHO	LAS	Fried	Fried et al. (2008)
Acetonitrile	$CH_3CN$	PTRMS	Wisthaler	Wisthaler et al. (2014)
Absorption coefficient dry, total, 532 nm	$b_{\text{abs}}$ , Abs_5	Nephelometry	Anderson	Wagner et al. (2015)
Scattering coefficient, dry, submicron 550 nm	$b_{\text{scat}}$ , Scat_5	Nephelometry	Anderson	Wagner et al. (2015)
Carbon monoxide	CO	LAS, GC	Diskin, Blake	Pfister et al. (2011)
Acetaldehyde	$CH_3CHO$	PTRMS	Wisthaler	Wisthaler et al. (2014)
Intensive quantities	Not proportional to carbon burned			
Single-scattering albedo	SSA	Nephelometry	Anderson	Wagner et al. (2015)
Ångström exponent, scattering	ÅE	Nephelometry	Anderson	Wagner et al. (2015)
Other variables used	$O_3$ , $NO_x=NO+NO_2$ , $NO_y$	Chemiluminescence, UV	Weinheimer (ARC-TAS), Ryerson (SEAC4RS)	Weinheimer et al. (1994), Ryerson et al. (2000)
Methane	$CH_4$	LAS, GC	Diskin, Blake	Pfister et al. (2011)
Methanol	$CH_3OH$	PTRMS	Wisthaler	Wisthaler et al. (2014)

Notes: PTRMS – proton transfer mass spectrometry; LAS – laser absorption spectrometry;  $1 - \omega$  is the single-scatter co-albedo; likewise, CO is linked to 1 (modified combustion efficiency) so that all values extend upwards from 0. For  $CO_2$  measurements, see text.

ing ratios but with  $b_{\text{scat}} > 2 \times 10^{-2}$  were allowed in. Plots of  $CH_3CN$  vs.  $b_{\text{scat}}$  suggested that a linear combination of the two minimal conditions clearly separated a population of forest fire plumes from other high-particulate situations.

There were forest fire plumes for which urban sources of CO and other fire tracers made attribution and quantification problematic, and so a further test based on CO was applied to exclude urban samples, using CO vs.  $CO_2$  plots for the years 2008 and 2013 separately (Fig. 2). We used a  $\Delta CO/\Delta CO_2$  ratio of  $< 33 \text{ ppb ppm}^{-1}$  to exclude plumes with excessive urban contamination. The figure suggests that some plumes with modest levels of urban influence remained and a few genuinely uncertain situations were excluded where fire might still have been dominant.

Species with sources other than biomass burning and with lifetimes sufficiently long to allow regional mixing can pose difficulties somewhat similar to  $CO_2$  variability, with solutions suggested in Sect. 8.2. We noted some localized observations of perplexing, consistently negative  $\Delta CH_4/\Delta C_{\text{tot}}$  relationships in the ARCTAS data (but not other species)

and removed these observation instances. Such relationships were found close to seaports or oil-producing regions.

### 3 Observed behavior of $C_{\text{tot}}$ in fire plumes – properties of tracers

This section provides some examples of  $C_{\text{tot}}$  and fire tracers. It illustrates the limitations of changes in  $C_{\text{tot}}$  along a sampling path as an indicator of fire influence,  $C_{\text{burn}}$ , for emissions estimation and the much greater similarities of the variations in tracers that possess shorter transformation time-scales. These define our approach to EnRs and EFs. The relation of fire emissions to observed  $C_{\text{tot}}$  to  $C_{\text{burn}}$  can be apparently simple or complex, depending on how the history of nonfire CO and  $CO_2$  entrained into fire plume air parcels affects  $C_{\text{tot}}$ . We show this commonality of relationships to motivate the theory of expanding plumes in Sect. 4. The theory suggests a regression relationship in Sects. 5 and 6, which applied, yields results in Sect. 7 that define relatively precise estimates of  $C_{\text{bkgd}}$ ,  $C_{\text{burn}}$ , and thus EnRs.

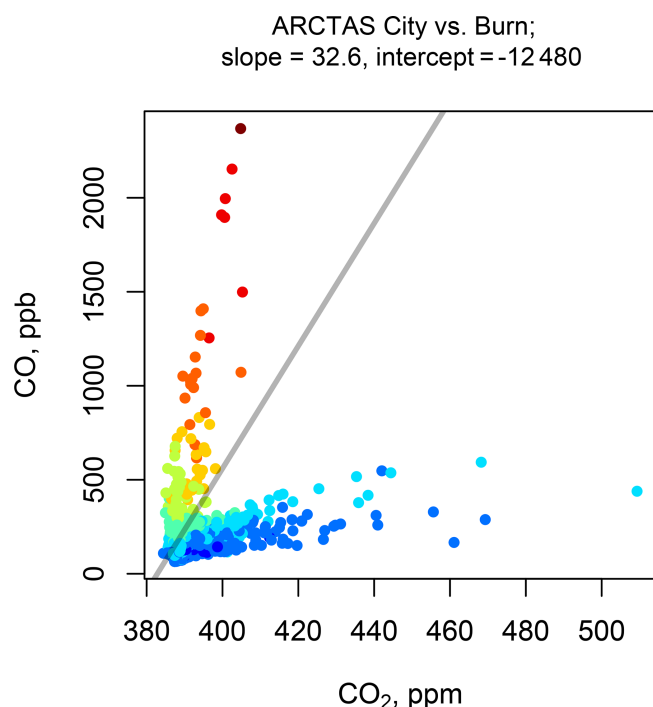


**Figure 2.** Urban and forest fire plumes are separable by the ratio of CO to CO<sub>2</sub>. Colors indicate a relative measure of CH<sub>3</sub>CN above the background, from blue (lowest, ~0.1 ppb) to red (highest, ~6 ppb) values. The straight gray line indicates our selected discrimination between nonurban and urban.

Figure 3 describes two flights in which plume encounters show how the interpretation of  $C_{\text{tot}} = C_{\text{burn}} + C_{\text{bgd}}$  can be simple or complex. Figure 3a shows the locations of the plume samples observed during SEAC4RS Flight 10 over Montana between 2 and 4.5 km a.m.s.l. Local topography ranged from 1 to 2 km elevation. This dataset included samples from the very intense plume of the Rim Fire (discussed later), collected far downwind. Figure 3b shows ARCTAS Flight 14, which was over the coastal mountains of Northern California at 0.5 to 1.5 km altitude, with topography from 0 to 1 km.

Figure 4a (whose sampling path is mapped in Fig. 3a) gives the time series of fire indicators from Flight 10. The fire tracers CO and  $b_{\text{scat}}$  appear generally well correlated with  $C_{\text{tot}}$ . This correlation is seen in Fig. 4b–c. Colors from blue to red give a key to sampling times. The large orange dots in Fig. 4a and d distinguish the plume points *selected* (based on our plume tracers) from adjacent nonplume measurements made in the flight. The lines connecting the adjacent plume samples suggest two or perhaps three linear patterns pointing back to a no-fire background of  $C_{\text{tot}} \sim 392.5$  and 394.5 ppm. Separately, a few points near the horizontal axis seem to suggest a low EnR. These points occur in the middle of sampling, just after 11:00 LT. Patterns of variation related to  $b_{\text{scat}}$  (550 nm, Fig. 4c) are very similar to those of CO (Fig. 4b). Most plumes encountered suggest very similar slopes.

Whereas the SEAC4RS data in Fig. 4a–c suggest mostly expected behavior, the ARCTAS Flight 14 measurements (Fig. 4d–f) show that  $C_{\text{tot}}$  variations, likely due to  $C_{\text{bgd}}$  variability, can greatly complicate the attempt to estimate EnRs. The very first samples plotted and those after about 13:35 LT have very clean tracer levels. (Those between 13:03 and 13:15 LT did not quite qualify as plume points, but the tracers do indicate some fire influence.) In this case, the trace of  $C_{\text{tot}}$  does not reflect fire influence well at all. Both fire tracers shown in Fig. 4d–f show wildly varying relationships to  $C_{\text{tot}}$  but are remarkably similar to each other in those relationships.

To conclude this section, we emphasize that variations in  $C_{\text{bgd}}$  do occur unexpectedly in many apparently homogeneous datasets. The lines composed of small black bars in both Fig. 4a and d use our results of Sect. 7; they are estimates of  $C_{\text{bgd}}$  for the selected fire plume cases. The patterns in Fig. 4 are given as plausible descriptions; the aim of this work is to support these with a uniform theory. For example,  $C_{\text{tot}}$  sampled by the airplane increases due to higher nonfire  $C_{\text{bgd}}$  from just before 13:00 to 13:15 LT and then decreases gradually until about 13:28 LT. At one sample around 13:21 LT and several at 13:20–13:30 LT, the background is particularly low, 382–383 ppm. This is a plausible description of the mixing of air masses with original concentrations of  $C_{\text{tot}}$  of ~382 and ~388 ppm. Wisps of less-mixed air occasionally interrupt a relatively continuing trend. A close examination of the CO and  $b_{\text{scat}}$  increments compared to  $C_{\text{tot}}$  increments in Fig. 4d–f agrees with this description suggested by the black dashes. The simpler case of SEAC4RS Flight 10 shows a similar example. At 11:08 LST, early in the flight, there is a brief excursion upwards of  $C_{\text{tot}}$  without any excursion in the tracers. The small black bars show this as a plausible excursion of  $C_{\text{bgd}}$ . Figure 4b and c show this as the two to three exceptional points, colored green, near the horizontal axis.

The plausibility of these examples highlights ideas of fundamental similarities in the way plumes of different tracers behave with entrainment even as  $C_{\text{bgd}}$  varies in response to distant, unrelated processes, as seen in Fig. 4a. This leads us to a mathematical description of our observations in Sect. 4.

## 4 Theory – expanding plume for several species

### 4.1 A general relationship

Figure 5 gives a general description of the dilution process, showing by the size of cubes how a mole of near-flame air is diluted by nonfire material as entrainment occurs. (The boxes shown suggest volumes, but lofting adiabatically changes volume. Discussion in terms of moles simplifies the discussion of mixing ratios and EnRs.) The figure is based on observations of plume size and plume dilution during rising followed by largely horizontal dilution downwind (Lareau and



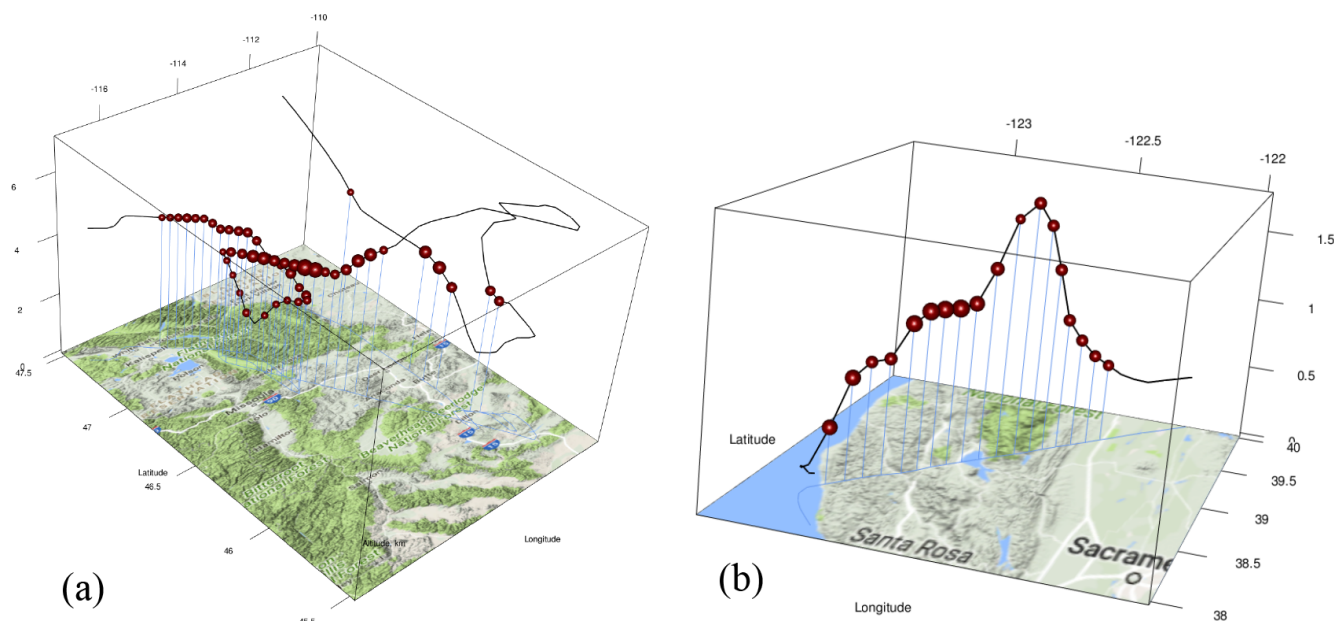


**Figure 3.** Flight paths and locations of plumes for two fire samples. **(a)** Sampling over Montana during SEAC4RS Flight 10. **(b)** Sampling in a cross-mountain transect along the Northern California coast. The size of the spheres indicates the relative amount of biomass-burning contribution. Numerical values of the contribution are in a later figure, Fig. 10. Some of the information was converted from © Google Maps using the R programming language.

Clements, 2017; Hanna et al., 1982), which are consistent with mixing ratios measured in this dataset and near-fire  $\text{CO}_2$  concentrations of  $1\text{--}2.5 \times 10^4$  ppm. The sizes are meant to be suggestive, but we found that they give a valuable frame of discussion for all lofted forest fire plumes. Some details are in the Supplement, “Note on Volumes”.

Using Fig. 5 as a guide, consider a parcel originating at a time  $t_1$  containing  $v = v_1$  moles that expands with an exponential relative rate  $r_v = v^{-1}(\text{d}v/\text{d}t)$ . (For our illustrative examples and to rationalize the MERET method, we need not start at the flame. We suggest a reasonable starting point described below.) This rate of expansion  $r_v(t)$  of the molar volume varies considerably over time, and fires are expected to have different magnitudes. Then molar mixing ratios will evolve with a law:

$$\frac{\text{d}x}{\text{d}t} = -\frac{1}{v} \frac{\text{d}v}{\text{d}t} (x - x^{\text{E}}), \quad (7a)$$

$$\frac{\text{d}y_j}{\text{d}t} = -\frac{1}{v} \frac{\text{d}v}{\text{d}t} (y_j - y_j^{\text{E}}), \quad (7b)$$

where  $x^{\text{E}}$  is the mixing ratio of entraining  $C_{\text{tot}}$  and  $y_j^{\text{E}}$  is the entraining background mixing ratio of fire tracer species or property  $j$ . (The term  $x^{\text{E}}$  here is later called  $x^0$  with a more general significance for possibly varying entrainment behavior.) The effect of volume addition is captured by  $v(t)$  which varies with time and expansion. The use of the relative rate  $v(t)$  does not require that the dilution is exactly exponential but does make the algebra somewhat simpler.

What happens when there are variable values of  $x^{\text{E}}(t)$  from fire to sampling point, for example in the boundary layer and free troposphere? Using  $\tau$  to describe the integration through time of an expanding parcel,

$$y_j(t_{\text{Sample}}) = \int_0^{t_{\text{Sample}}} -v(\tau) (y_j(\tau) - y_j^{\text{E}}(\tau)) \text{d}\tau + y_j(t=0), \quad (8)$$

with a similar equation for  $C_{\text{tot}}$ , which can be called  $x(t_{\text{Sample}})$ . It involves  $x(\tau)$  and  $x^{\text{E}}(\tau)$ , where  $x(t=0)$  and  $y_j(t=0)$ . These are determined by the  $C_{\text{burn}}$  from the fuel consumed and the tracer compounds released at the same time, as well as by background concentration,  $C_{\text{bkgd}}$ , and pre-flame backgrounds of the tracer  $y_j^{\text{E}}$ . We leave aside as a separate problem for a fire-burning model the complexities of the actual flame and its incorporation of additional air. Our point  $t=0$  is when entrainment of nonburning air becomes dominant.

Given the realities of atmospheric sampling, we must avoid describing the complete history of  $v(\tau)$  and any complex variation in  $x^{\text{E}}(\tau)$  and  $y_j^{\text{E}}(\tau)$ . This would require a complete description of air along the parcel trajectory and the turbulent physics of entrainment. Rather, we provide simple illustrations showing how generally the entrainment process affects both  $x(\tau)$  and all the  $y_j(\tau)$  values in the same proportions. This is a single-parcel description ignoring complexities of the rest of the plume. For convenience of discussion,



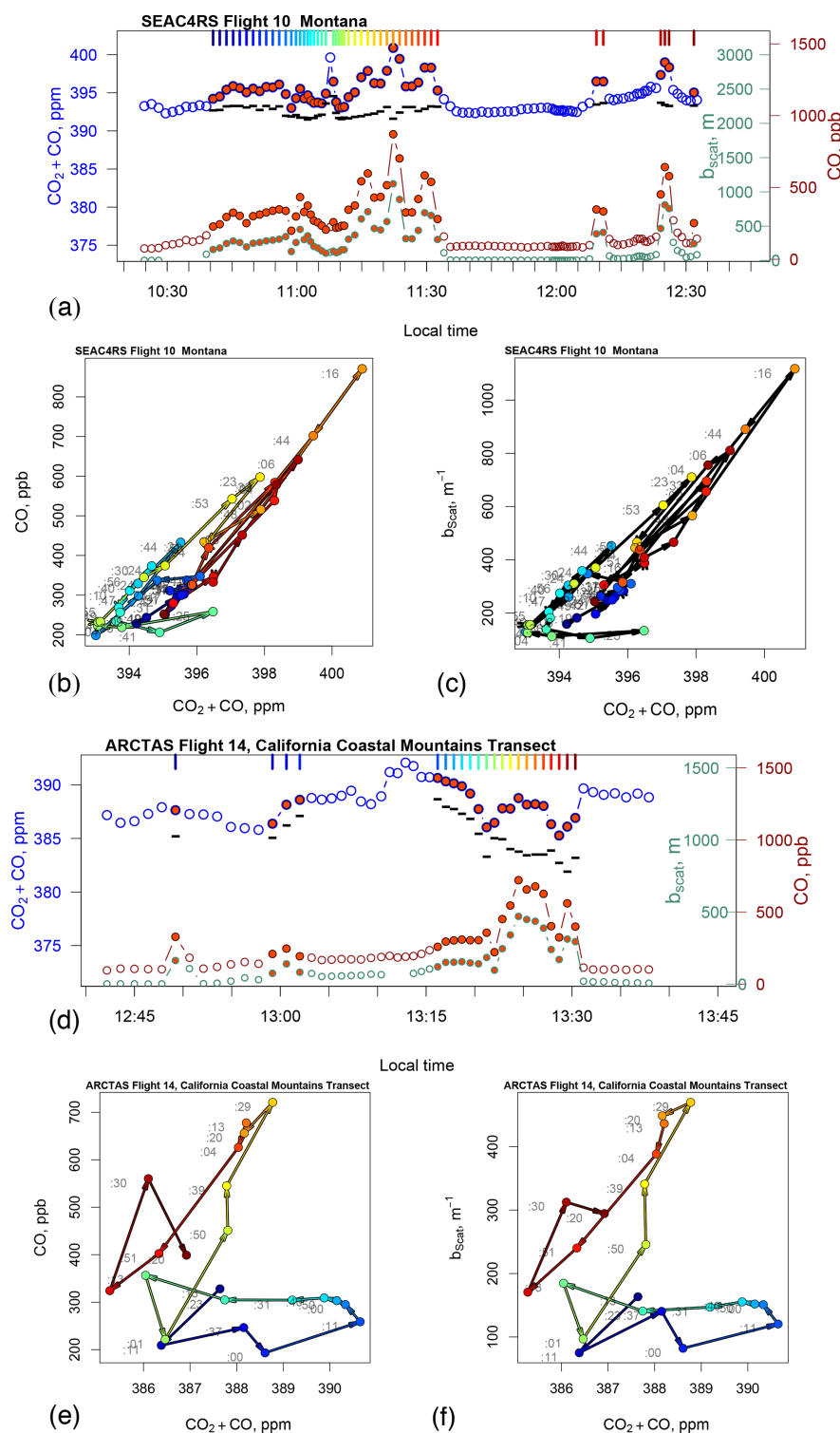


**Figure 4.** (a) Timeline of sampling, for the period shown in Fig. 3a, Montana, of  $\text{CO}_2 + \text{CO}$  (blue, left axis) and the fire tracers  $\text{CO}$  and  $b_{\text{scat}}$  (red and green points, right axis). Orange-filled points were identified as clear plume points. Unfilled points were not identified as such but might have some fire influence, especially near plume points. (b) Scatter diagram of  $\text{CO}$  vs.  $\text{CO}_2 + \text{CO}$  with arrows showing the time progression of aircraft sampling of identified plume points. Colors provide a key to times shown in panel (a). Light gray numerals give observation times in minutes. (c) A similar diagram of  $b_{\text{scat}}$  vs.  $\text{CO}_2 + \text{CO}$ . Similar shapes of figures are noted in the text. (d) Timeline of sampling for the period shown in Fig. 3b, coastal transect. (e) Scatter diagram of  $\text{CO}$  vs.  $\text{CO}_2 + \text{CO}$  during the transect, like in panel (b). (f) A similar diagram of  $b_{\text{scat}}$  vs.  $\text{CO}_2 + \text{CO}$  for the coastal transect. The black bars graphed in panels (a) and (d) are estimates of nonfire-influenced  $C_{\text{bgd}}$ ; see text. They and the nonplume points suggest air mass changes in  $\text{CO}_2 + \text{CO}$ .



**Figure 5.** Inflow of air into an expanding fire plume; a likely near-fire aircraft sampling location would be near the cube on the upper right. Cubes are shown with 3-D sizes proportional to the number of moles of entrained air. These may be considered volumes of air adjusted downwards to compensate for the adiabatic expansion that rising plumes undergo. The smallest cube is taken to be near the flames, at roughly the point where fire emissions transition from mixing to entraining background air. Exact placement of this cube is not important to the analysis of entrainment, expansion, and tracer mixing ratio. Successively larger cubes have volumes roughly in the ratio of 1, 40 (partially raised), and 140 (near-neutral buoyancy level); sizes are consistent with a buoyant fire plume (Lareau and Clements, 2017). The rightmost cube has a ratio to the first of 400, consistent with horizontal Gaussian dispersion during travel downwind. See text for more details.

we will describe cases in which the environmental air entrained has one or two values each of  $x^E(\tau)$  and  $y_j^E(\tau)$  that are constant over long periods. For example, the background concentration of  $x^E = C_{\text{tot}}$  often has one value in the mixed layer and a different value above the mixed layer, potentially taking on several values in several layers. The same is true for the fire tracers  $y^E$ . Conceptually there may be several regions which contribute; the exact history is lost. Our idea is that regression analysis allows us to infer a characteristic sum of effects which is described by a single quantity. The analysis can only be as complex as the number of our measured quantities allows. See also Supplement, “Note on Initial Point”.

Returning to the differential-equation view of the simple expanding plume model, we see a method for estimating the most important parameters. Solving each of the equations for the expansion rate and equating the expressions, we obtain a form that eliminates the details of entrainment and emphasizes proportionality. We recommend the reader to refer to Table 2 during the discussion of theory and then the discussion of estimation details.

$$\frac{1}{(y_j - y_j^E)} \frac{dy_j}{dt} = -\frac{1}{v} \frac{dv}{dt} = \frac{1}{(x - x^E)} \frac{dx}{dt} \quad (9)$$

Since  $dy_j^E/dt = 0 = dx^E/dt$ , we get

$$\ln(y_j - y_j^E) = \ln(x - x^E) + C_j, \quad (10)$$

$$(y_j - y_j^E) = a_j (x - x^E) a_j = \exp(C_j). \quad (11)$$

Note that by our definitions, the reasonable interpretation of  $C_j$  is the EnR  $a_j$  for species  $j$ .

Consider two observations of the same plume, each made at differing degrees of dilution  $v$ . For convenience, these are labeled  $\beta$  and  $\alpha$ , mnemonically “before” and “after.” Temporally they could be nearly coincident or  $\beta$  could come after  $\alpha$ .

$$(y_{\alpha j} - y_{\beta j}) - (y_j^{E\alpha} - y_j^{E\beta}) = a_j (x_\beta - x_\alpha) - a_j (x^{E\alpha} - x^{E\beta}), \quad (12)$$

for periods of expansion in which the entrained concentrations are constant. See also Supplement, “Note on Varying Entrainment”.

This formula is the basis for the NEMR technique mentioned above, with  $j = \text{CO}$  playing a particularly important role. The inequality restrictions should be evaluated for an EnR to be a candidate for an ER and then an EF. In some cases, the background values,  $x^{E\alpha}$  and  $y_j^{E\alpha}$ , might be estimated from measurements made outside the plume. It can be somewhat more difficult to estimate  $x^{Eb}$  and  $y_j^{Eb}$  upwind of the source, especially for air entraining into the fire plume at its source. A plume may also entrain air from various backgrounds and at various times during lofting and spread. That is, the history of entrainment may well be more complex than two conditions, “a” and “b”, and the number of situations where we may estimate EnRs and then EFs is greatly limited. This important realization was described by Yokelson et al. (2013). The NEMR method can deal with most differences in  $x^{Eb}$  but not in  $y_j^{Eb}$  for most tracers, and the quantity

**Table 2.** Table of symbols.

Symbol	Definition	Observed, estimated, or hypothetical	
$C_{\text{tot}}$	$\text{CO}_2 + \text{CO}$ (+ other carbon, ignored here), parts per million.	O	
$C_{\text{burn}}$	$\text{CO}_2 + \text{CO}$ (+ other carbon, ignored) emitted from fire, present downwind, in plume sample, to be estimated as $(x_i - x_i^0)$ .	E	
$C_{\text{bkgd}}$	$\text{CO}_2 + \text{CO}$ <i>not</i> emitted from fire, present downwind in plume sample, thought of as a mixture of $C_{\text{tot}}$ entrained at various stages in plume expansion and rise. The background may be assumed for illustration or computed from the estimated $x_i^0$ . This is not necessarily air surrounding the plume sample.	E	H*
$C_{\text{bkgd}}^{\text{Approx}}, v_i$	Early approximate $C_{\text{burn}}$ ; a rough rescaling from the unitless burn-normalizing variable $v_i$ to parts per million, often a convenient guide and check.	E	
$C_j$	A constant of integration, replaced by $a_j = \exp(C_j)$ .		H
$i$	Sample sequence number, organized for convenience by time of the sample.	O	
$j$	Tracer number for regression, in this work 1 to 8 or “CO” or “ $b_{\text{Scat}}$ ”, etc. After regression estimation is completed, $j$ may be used similarly to specify any fire emission concentration or response, e.g., “propene” or “ $\text{O}_3$ ”.	O	
$a$ or $b$	Location at beginning or end of a period of idealized plume development and entrainment.		H*
$x$	$C_{\text{tot}} = \text{CO}_2 + \text{CO}$ considered as a continuous variable.		H
$y_j$	Tracer concentration of fine tracer variable $j$ , e.g., toluene, $b_{\text{Scat}}$ , considered as a continuous variable.		H
$x_i$	Vector components of $C_{\text{tot}} = \text{CO}_2 + \text{CO}$ describing a plume sample location and time $i$ , used in algebraic development, shown on $x$ axis.	E	H*
$y_{ij}$	Array components of $C_{\text{tot}} = \text{CO}_2 + \text{CO}$ describing tracer concentration of fire tracer variable, $j$ , e.g., toluene, $b_{\text{Scat}}$ , at plume location and time $i$ .	O	H*
$x^{\text{Ea}}$ or $x^{\text{Eb}}$	Environmental air “background” $C_{\text{tot}}$ concentrations existing at location $a$ , i.e., the beginning of our integration of the plume expansion equation. $b$ signifies condition at the end of calculation.		H*
$y_j^{\text{E}}$ or $y_j^{\text{Ea}}$	Background concentration of tracer $j$ . Typically estimated as a minimum value from observed probability density function for samples in a particular flight mission, especially nonplume samples without signals of stratospheric air.	E	
$a_j$	Slope relationship of $y_{ij}$ to $x_i$ for species $j$ , typically species $j$ under burning conditions for a “fire type” that is common for all species at instance (time) $i$ . These slopes then transform to EnRs and ERs.	E	
$c_j$	Intercept relationship of $y_{ij}$ to $x_i$ .	E	
$y_{ij}^0$	$y$ intercept implied by $x_i$ , $y_{ij}$ , and the estimated slopes $a_j$ for $j$ .		
$\hat{x}_{ij}^0$	One of several (10) estimates of $x_i^0$ based on tracer $j$ and fire type assigned by clustering for observation instance $i$ .	E	
$\hat{x}_i^0$	The median of the $\hat{x}_{ij}^0$ over all the tracers $j$ .	E	
$(x_i - x_i^0)$	The estimate of $C_{\text{burn}}$ for instance $i$ in theoretical development and then from regression. Regression results are properly $(x_i - \hat{x}_i^0)$ .	E	

\* Note that symbols may transition from hypothetical to estimated as the discussion develops.

$y_{\text{CO}}^{\text{Eb}}$  for carbon monoxide must be well sampled and well understood.

#### 4.2 Examples showing robustness of computations of idealized $C_{\text{tot}}$

We used this approach to produce the following concrete examples of increasing complexity. They illustrate the origin of the features seen in Fig. 6 in terms of this simple plume dilution model. They helped motivate our solution techniques and indicate methods of analysis of individual plumes. These examples indicate possible limitations, but they also indicate a comforting averaging behavior of the linear differential equations as they describe our solutions. These uniformities and deviations also showed up in the analyses that we develop below. The examples also give some quantitative feel for the effects of deviations from the simplest hypothesis; e.g.,  $x^{\text{E}}$  and  $y_j^{\text{E}}$  remain constant through time. Fig. 6 shows calculations describing behaviors of  $x$  and  $y_j$  in several plausible situations. Each graph represents the development of plume mixing ratios for a period of plume doubling, similar to the analysis time chosen in Poppe et al. (1998), following their equations, Eqs. (7) and (8). The dots show equal increments of plume expansion. Most parameters defining the equations may be read from the graphs themselves. Each initial concentration is shown by the points to the upper right of the line, i.e., the points with maximum  $x = C_{\text{burn}}$  and  $y_j = \text{tracer concentration}$  for each case considered.

Figure 6a illustrates a plume history for  $x^{\text{E}} = 380$  ppm and EnRs with respect to airborne  $C_{\text{tot}}$  of  $95 \times 10^{-3}$ ,  $12 \times 10^{-6}$ , and  $25 \times 10^{-6}$  ppm ppm<sup>-1</sup>, which are reasonable values for carbon monoxide (in ppb), benzene, and ethylene (in ppt). In the figures, focus attention on the relative behavior of the tracers. It is assumed that there are no consequential production or destruction reactions and also that there is a constant background tracer concentration, which has been subtracted. The individual plots show situations of increasing complexity. Figure 6a shows the dilution behavior of the three species. A constant dilution rate is plotted; note that a varying dilution rate changes the spacing of the dots but not the linear pattern. Larger dots highlight an equivalent dilution of tracer and  $x = C_{\text{tot}}$  as would be observed in hypothesized discrete airplane samples. Figure 6b illustrates the dilution of CO in environments with differing entrained  $x^{\text{E}}$ . In Fig. 6a the larger dots align vertically; in Fig. 6b, they align horizontally. Figure 6c illustrates the situation where both EnRs and backgrounds vary; the thin lines emphasize independent aspects of EnR and  $x^{\text{E}}$ . The points on the  $x$  axis where (excess) tracer is zero are important to our estimation technique, more important than  $x^{\text{E}}$ . Estimation of  $x^{\text{E}}$  utilizes data on the vertical lines, while EnRs utilize information from both the vertical and the horizontal lines. Statistically speaking, the problem of estimation of both backgrounds and EnRs illustrates simultaneous effects that are “separable”. The reader may wish to extend the analysis to a large sequence of changes

in entrained concentrations and note the essential linearity of this aspect of the formulation and that the solution expresses an appropriate averaging effect. We remark that the near uniqueness of the solutions obtained below (making small allowances for measurement error) will underline the robustness of the solutions.

However, the effect of uniform variations in background tracer concentrations  $y_j^{\text{E}}$  is not completely solved in this work.  $y_j^{\text{E}}$  can be estimated by examining the lowest values of  $y_j^{\text{E}}$  in nonplume air; it is best to exclude values that appear to have contributions of exotic air (e.g., stratospheric air) or possible measurement problems at very low mixing ratios (e.g., negative values). Some comments follow as we move towards the topic of estimating individual values from a large set of  $x_i$  values and  $y_{ij}$  values in a practical situation where we analyze instrumental data. Restricting attention to larger values of  $x_i$  and  $y_{ij}$  greatly ameliorates problems arising from  $y_j^{\text{E}}$ .

#### 5 Theory – a regression relationship for EnRs

Let us consider more broadly the equations that provide a basis for statistical estimation. For current purposes of explanation, we make the seemingly large assumption that points from different plumes have similar properties at the same degree of dilution and may be compared. That is, the  $a_j$  values are consistent for all plumes. Effects of varying  $x^{\text{E}}$  and  $y_j^{\text{E}}$  between the plumes may be largely taken out by regression; that is our current concern. Later, we will describe our approach to address possible variations in the EnR relationships  $a_j$  for parcels in the same or different plumes.

The basis of MERET utilizes the concept of the unmeasured extreme where  $y_{aj} = 0$ . To begin with, we consider the situation where (i) the emissions relationships  $a_j$  are constant for all observations and (ii) background values of the tracers are small enough in a relative sense; i.e.,  $|y_j^{\text{Ea}} - y_j^{\text{Eb}}| \ll |y_{aj} - y_{bj}|$ . That condition is common for many species that have loss timescales of less than a month and/or have small nonfire sources. Each of these restrictions can eventually be relaxed. In this case

$$y_a = a_j \left( x_a - \left\{ x_b - x^{\text{Eb}} + x^{\text{Ea}} \right\} \right) + y_j^{\text{Ea}} - y_j^{\text{Eb}}, \quad (13a)$$

$$y_a = a_j \left( x_a - \left\{ x_b - x^{\text{Eb}} + x^{\text{Ea}} \right\} \right),$$

$$\text{for } |y_j^{\text{Ea}} - y_j^{\text{Eb}}| \ll |y_{aj} - y_{bj}|. \quad (13b)$$

Notice that terms within braces can be estimated by regression as sums, varying by the situation  $b$ . What if the values of these terms change discretely in time, for example as a plume leaves a daytime mixed layer or distinct upper-air plumes are encountered? Simple algebra with linear formulas suggests that estimates of the terms in braces change discretely. Grad-

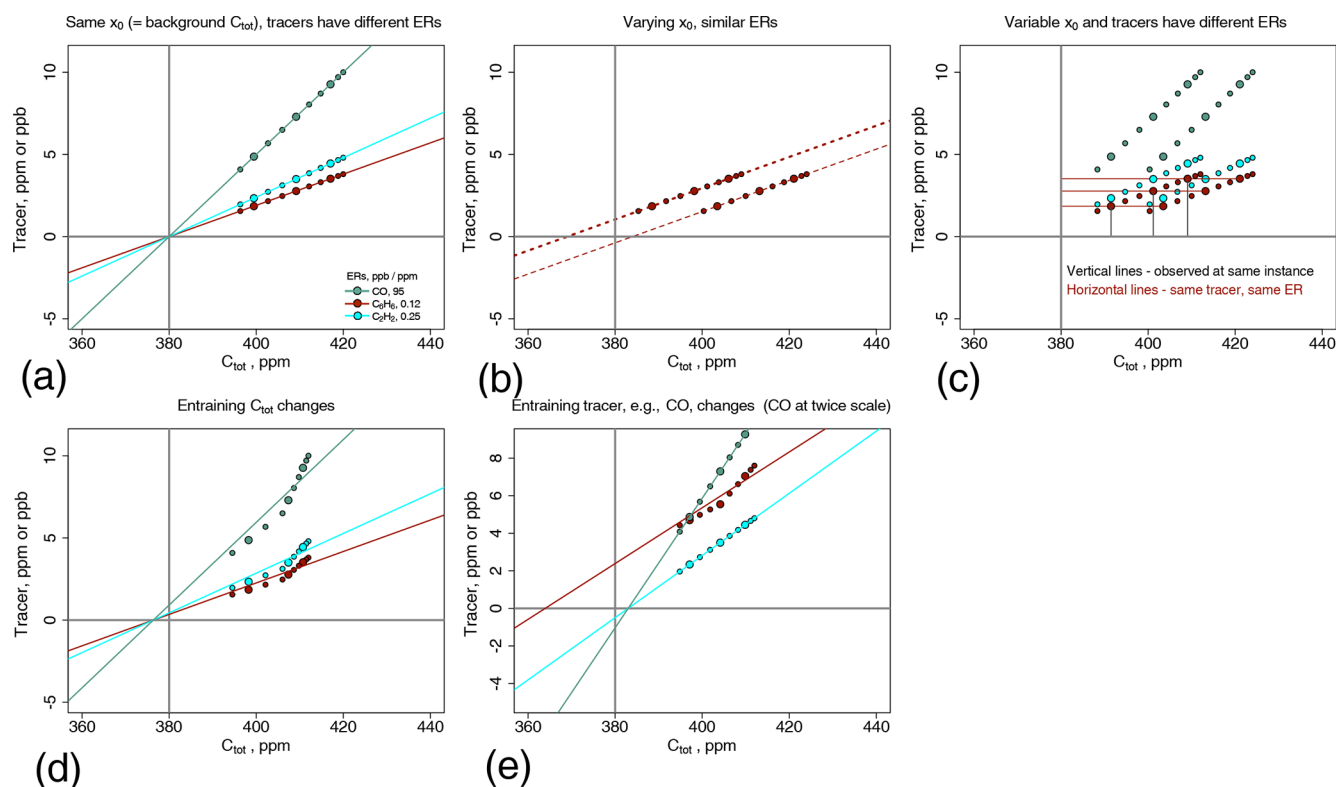


**Figure 6.** (a) Simulated dilution of three different fire tracers' EnRs as shown, and with environmental  $x^E$  of 380 ppm. These are nominally CO, benzene, and ethylene. Background concentrations of the tracers have been subtracted.  $C_{\text{burn}}$  is measured from the y axis, where  $C_{\text{tot}}$  has the value of 380 ppm. Larger dots highlight equivalent degrees of dilution. (b) Simulated dilution of one tracer, nominally CO above background, with different background  $x^E$ . Backgrounds are illustrated by the  $x$  intercepts. (c) Simulation of three tracers, varying EnRs and varying backgrounds (deducible from the  $x$  intercepts). Thin lines emphasize similar constant  $y$  values with different backgrounds and constant  $x^0$  values with varying EnRs. (d) Simulations like in panel (a) but with a change in the  $x^E$  entrained  $x^0 = C_{\text{burn}}$  background from 395 to 375 ppm at the time of the eighth dilution step. A single applicable background value of  $\sim 378$  ppm is a linear interpolation between 395 and 375 ppm. (e) Simulation where background  $x^E$  remains constant but background CO changes by 1.5 ppb during the same time (CO drawn at twice the height for visibility).

ual changes in entrained mixing ratios of course imply a continuity condition on these terms.

We return to the illustrative dilution behaviors described in Fig. 6. Figure 6d describes a sudden change in background  $x^E$  by 20 ppm,  $x^{Eb}$  to  $x^{Ea}$ , midway in the expansion and dilution; at this stage of plume evolution, 20 ppm is about 4 times larger than typical fire contributions to  $C_{\text{tot}}$ . Estimates of  $x_i^0$  from a few samples along these lines (without knowledge of the time of change) would be intermediate. Equation (13) suggests that the EnR estimate need not be affected. Some similar calculations make it clear that the estimates average satisfactorily under varied assumptions. Figure 6e shows a very contrasting behavior, when there is a sudden change in concentration of entraining tracer (CO) during plume dilution, a change of 1.5 ppm. In comparison, the addition of CO by burning at the start of the interval is  $\sim 3.5$  ppm. We may distinguish this as  $\hat{x}_{ij}^0$ , where the  $j = \text{CO}$  and the hat indicates an estimate. This graph also suggests that if there are more than three tracers (we use eight), then the median of

all the estimates, median ( $\hat{x}_{ij}^0$ ), is robust against errors resulting if a tracer  $j$  has a variable or poorly described background, resulting in  $\hat{x}_{ij}^0$  at falling being distinctly higher or lower than the others. We must be concerned about this since tracers can have occasionally important nonfire sources. A small change in background of a tracer compared to observed change due to fire is critical in determining a useful estimate of the background  $x^0$  as well as in determining the quality of the EnR of a tracer. Methane in particular has a long atmospheric lifetime and several sources of similar strength; in California, livestock and fossil-fuel extraction significantly influence mixed-layer concentrations flowing into a fire up-draft. Consequently, it can exhibit variations that are more than 10 % of the fire emission contribution for well-dispersed plumes.

The preceding discussion suggests that we may use the specialized least-squares technique,

$$y_{ij} = a_j (x_i - x_i^0) + e_{ij}, \quad (14)$$

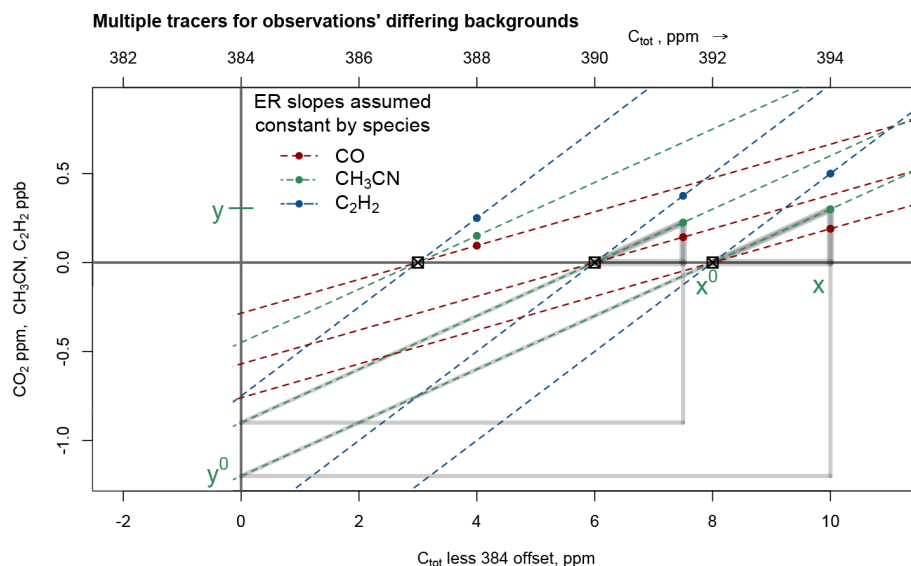


**Figure 7.** Multiple tracers allow a solution for an equivalent-background  $x^0$  value, illustrated by an idealized example largely replicating the conditions of fire plume sampling above an Amazonian mixed layer as described by Yokelson et al. (2013). The dashed colored lines indicate the theoretical response of tracer to the  $C_{\text{tot}}$  when  $C_{\text{bkgd}}$  takes on various values indicated by black squares. There are several lines showing the ideas expressed in Fig. 6a. The fact that the various colored lines associated with each  $x$  value meet at the value with  $x$  coordinate  $x^0$  and  $y$  coordinate 0 represents the estimation that precisely solves Eq. (5) above. If we had included error in observations or variation in EnRs, there would be variations in the positions of  $x^0$  and the slopes. As Sect. 6.1 describes, regression of tracer vs.  $C_{\text{tot}}$  is required and gives a spread of  $y$  intercepts. Nevertheless, these can be mapped back to  $x$  intercepts using slopes and the concept of similar triangles. The nested gray triangles illustrate this idea for each of two values of  $x^0$ .

where the  $x_i$  and the  $y_{ij}$  are observations of  $C_{\text{tot}}$  at an instance  $i$  and for the set of variables  $j$  at that instance  $i$ . Here  $x_i^0$  expresses several terms of Eq. (13) and any other corrections not proportional to  $a_j$ . We may call  $x_i^0$  an “effective background”. However, it is not a specific background but actually summarizes the whole effect of changes in  $C_{\text{bkgd}}$  and also the degree of dilution. This means that the regression can synthesize information from not just one well-characterized plume but also different plumes provided we expected them to have similar  $a_j$  behavior. Figure 7 illustrates the use of regression employing the ideas developed in Fig. 6. Using the same formulas as above, we depict observations of CO,  $\text{C}_6\text{H}_6$ , and  $\text{C}_2\text{H}_2$  made at three instances (times). The three tracers determine a value  $x^0$ , and given that information, the three tracer enhancements and therefore tracer EnRs are determinable. The nested gray triangles, similar triangles, illustrate this idea for each of the two values of  $x^0$  corresponding to two observation instances when it is assumed that  $x^0$  has changed. MERET uses the idea that the slopes must be equal. This simulation assumes no error in the measurements of  $\text{CO}_2 + \text{CO}$  or the tracers and assumes no variation in the EnRs, so values are determined perfectly.

How well are these situations with multiple observation instances and multiple tracers determined? In the case of two samples and two tracers, i.e.,  $N_{\text{Instance}} = 2$  samples and  $N_{\text{Tracer}} = 2$  slopes (EnRs), we need to estimate  $x_1$ ,  $x_2$ ,  $a_1$ ,  $a_2$ , and  $x_0$  using only  $y_{11}$ ,  $y_{12}$ ,  $y_{21}$ , and  $y_{22}$ ; there are not enough

measured variables to determine a unique solution:  $N_{\text{Tracer}} + N_{\text{Instance}} + 1 > N_{\text{Tracer}} \cdot N_{\text{Instance}}$ ; viz.,  $5 > 4$ . However, if there are three tracers,  $N_{\text{Tracer}} \cdot N_{\text{Instance}} > N_{\text{Tracer}} + N_{\text{Instance}} + 1$  and we get a solution. In this case, any measurement error, or indeed lack of perfect similarity in response slopes, can give somewhat conflicting solutions.

## 6 Methodology

### 6.1 Finding the $\text{CO}_2 + \text{CO}$ background

The use of tracers with backgrounds removed and then scaled to a common mean establishes a well-conditioned matrix problem and easier analysis of sensitivity effects. We have identified forest fire plume samples and  $N_{\text{Tracer}}$  tracers whose background values can be reasonably estimated. Let us proceed with the regression and begin to address some complications that arise. The mathematical problem we must solve is Eq. (14), which we will rewrite to emphasize that we are starting in native units.

$$y_{ij}^{\text{measured}} - y_j^{\text{E}} = a_j (x_i - x_i^0) + e_{ij}$$

In the following development in this section, we will work with  $y_{ij}$  above the background; i.e., set  $y_{ij}^{\text{prenormalized}} \leftarrow (y_{ij}^{\text{measured}} - y_j^{\text{E}})$ .



We must attempt to fit  $y_{ij}^{\text{prenormalized}}$  for each species  $j$  (1 to  $N_j$ ) and for each measurement instance  $i$  (1 to  $N_j$ ). The term  $e_{ij}$  describes the error. Besides removing backgrounds, we wish each tracer  $j$  to contribute equally to the sum of squares that determines a regression, independent of the tracer's mean value. Consequently, we should normalize the tracers so that their mean is 1:

$$y_{ij} = y_{ij}^{\text{prenormalized}} / \text{mean}_i(y_{ij}^{\text{prenormalized}}).$$

We will use normalized values of the tracers for the following development until Eq. (20). It is not necessary to normalize  $x_i$ , but it will be useful to subtract a baseline. This suggests that the basic regression equation might be the following:

$$y_{ij} = a_j (x_i - x_i^0) + e_{ij}. \quad (15)$$

Equation (15) also summarizes just why the determination of ERs is difficult: the equation is nonlinear in the multiple regression sense; i.e., we must include the mixed  $i$  and  $j$  term  $a_j x_i^0$  as a regression term. The problem is a mixed-effects model: we must estimate the statistics of two separately varying processes affecting  $x_i^0$  and  $a_j$ .

A complication arises concerning the use of regression. The fire tracer variable  $y_{ij}$  values must “point back” to a zero point, where no  $C$  was added by the burn,  $C_{\text{burn}} \equiv x_i - x_i^0 = 0$ , but each instance  $i$  may have a different zero point. A regression formula should solve this in some way. Commonly, regression fits provide a  $y$  intercept, i.e., the value at  $x = 0$ . Here we have an  $x$  intercept to estimate, i.e., the concentration of the reference species at zero-added fire emissions, and so the problem becomes nonlinear in the regression sense. In summary, we have a nonlinear random-effects model (Pineiro and Bates, 2000; Gajoux and Seoighe, 2010; Bates et al., 2014; Gajoux, 2014), which requires specialized techniques.

One feature of Eq. (15) is emphasized: the formulation does not require any relationship of  $x_i$  or  $y_{ij}$  in time; instances must only represent a sufficiently coherent class of fires. One would expect more accuracy and discernment of features in similar forest fires but not in forest fires and grass fires. For the latter case, the assumption of consistent  $a_j$  becomes problematic.

Why not simply reverse the problem and seek  $x$  as a function of  $y$ ?

$$x_i = \alpha_j y_{ij} - x_i^0 + e_{ij}, \quad (16)$$

where  $x_i^0$  values are estimated with a regression model (specifically a fixed-effects model). The difficulty is that the trivial solution  $x_i = -x_i^0$  fits perfectly and was hard for us to avoid even when we attempted to restrict the solution with a nonlinear solver. Is it not easier to convert  $y$  intercepts into  $x$  intercepts? This appears more productive and should appeal to those not familiar with using a nonlinear solver in

this particular mode of nonlinearity. In place of Eq. (15), we may write a regression equation with an intercept:

$$\text{Regress } y_{ij} = a_j x_i + c_i^0 + e_{ij}, \quad (17)$$

where the  $y$  intercepts,  $c_i^0$  values, are estimated for each instance and the  $e_{ij}$  values are minimized by least squares. The R expression used to solve this problem was `main.lmer = lmer(y ~ x + (x - 1 | species.type) + (1 | id) + 1)`, where `id` indicates the sequential observation number for the tracer species. The term `species.type` indicates the species description  $j$ . The word `type` signals a generalization described in the next section. (This expression is written in a commonly used Wilkinson–Rogers symbolic form: the symbol  $\sim$  describes our intention to make a regression estimate; Wilkinson and Rogers, 1973. The vertical lines indicate how factors are involved with variables; 1 indicates an intercept is to be described by a random effect; and  $(x - 1 | \text{species.type})$  indicates that a slope that multiplies  $x$  is to be estimated, indexed by `species.type`. “No intercept estimated” is signaled by  $-1$ .) The regression results generate a set of fitted  $y$  values which we may call  $\hat{y}_{ij}$  and a set of fitted  $\hat{a}_j$  values. Together, the values of  $x_i$ ,  $\hat{y}_{ij}$ , and  $\hat{a}_j$  imply a  $y$  intercept  $y_{ij}^0$  when  $x_i = 0$  as shown in Fig. 7. One evaluates the fit for  $x_i = 0$ . Then one may use the slope estimate  $\hat{a}_j$  of  $a_j$  by regression to find the several estimates of  $\hat{x}_{ij}^0$  provided by

$$\hat{x}_{ij}^0 = (\hat{y}_{ij} - y_{ij}^0) / \hat{a}_j. \quad (18)$$

This is where we use the similar-triangles concept of Fig. 7. The use of a single  $\hat{a}_j$  value for all observation instances of the same species (more precisely, `species.type`) is a strong constraint on the resulting estimate. This is how for  $\hat{a}_j$  and  $\hat{x}_{ij}^0$  we use the concept of the similar triangles described in Fig. 7 of Sect. 5.

We then take

$$\hat{x}_i^0 = \text{median}_j \hat{x}_{ij}^0. \quad (19)$$

The estimation of  $\hat{x}_i^0$  now allows estimates of the incremental carbon liberated to the atmosphere,  $C_{\text{burn}} = (x_i - \hat{x}_i^0)$ . We will drop the hat from  $\hat{x}_i^0$  below, writing  $x_i^0$  and  $C_{\text{burn}} = (x_i - x_i^0)$  except when we wish to emphasize their nature as estimates. Emission factors for individual-tracer species may be obtained directly by adding fixed and random effects on slopes for each species and each observation,  $\hat{a}_j$ . An enhancement ratio for any concentration or property  $y_j$  with a background, measured at time  $i$  in the aircraft sampling, can be obtained using the carbon-burned estimate:

$$\begin{aligned} \text{EnR for } y_{ij} &= \frac{(y_{ij}^{\text{measured}} - y_j^{\text{E}})}{(x_i - x_i^0)} \\ &\equiv (y_{ij} - y_j^{\text{E}}) / (C_{\text{burn}})_i. \end{aligned} \quad (20)$$

To repeat, the variable  $y_{ij}$  now stands for any property for which we seek an EnR, for example ozone, which is not one of the eight indicator variables.  $y_j^E$  describes a non-fire-dependent background value. This ratio estimate is available for all tracers and is preferred over a similar slope variable  $\hat{a}_j$  used to estimate  $x_i^0$  in the in Eq. (18) above.

Formulas for the statistics of ratio quantities with uncertainties in the numerator and denominator can be theoretically complex, so we simply computed error estimates by simulation using computed Bernoulli trials. For both the numerator and the denominator, 1000 samples of normal distributions were calculated, using their uncertainties as  $1\sigma$  values. Then the ratios of the first numerator and first denominator normal deviate sample, the second, ..., the 1000th normal deviate sample for the numerator divided by the 1000th normal deviate sample were calculated, and the distribution of ratios was summarized. For the numerator, the measured value and the suggested standard deviation (typically a percentage ratio) provided the parameters for the normal distribution. For the denominator, the mean was the  $C_{\text{burn}}$  estimate, and the standard deviation was a value of 0.25 ppm, documented as the measurement error (precision + bias) of  $\text{CO}_2$  (see Table 1). Uncertainties in the calculation of  $\hat{x}_i^0$  were considered small and did not add to the dispersion of the denominator, especially since it is clear that any additive biases contributing to the quoted uncertainty in  $(\text{CO}_2 + \text{CO})$  cancel out. Sample calculations in the Supplement (“Note on Sensitivity to Number of Tracers Used”) suggest errors typically of a magnitude of 0.03 ppm due to variations in technique and usually of  $< 0.1$  ppm. Additive errors should also cancel out for the numerator, since a background is subtracted. Indeed, some tracers like ethene appeared to have a negative background as determined from plots and simple regression calculations of  $y_{ij}$  on  $(C_{\text{burn}})_i$ . This is not unexpected, since these compounds are sampled into cans, where a small but self-limiting coating of the measured species on the can surfaces might cause such a negative offset, and yet the integrity of the can sample at larger values might be little affected.

## 6.2 Practicalities – variable EnRs

Equations (17)–(19) provide the basis of MERET. There are however some details that increase its relevance and accuracy. First there is normalization. Common practice is to normalize all the tracer species  $j$  with respect to the mean of all observations of species  $j$ , after subtracting a baseline. This allows each tracer to influence  $y_{ij}$  equally. Assigning weights accomplishes the same purpose, but scaling allows better diagnostic graphs. In fact, the literature referenced above emphasizes how informative  $j = \text{CO}$  is, despite its relatively small variation in EnR or slope. Consequently, we give CO twice the weight of all the other species.

Secondly, we allow for a certain amount of true variation in the EnRs, expecting this to make Eq. (18) perform better. This is done by imagining that virtual species can be asso-

ciated with “fire types”, for example “flaming CO”, “smoldering CO”, or “high-nitrogen-fuel  $\text{CH}_3\text{CN}$ ”. A fire type is a value for each observation that applies to all tracer species at that instance. It expresses commonalities between different mixes of burning emissions, commonalities that may be more frequently or less frequently expressed in any given plume, e.g., smoldering-CO fire type. We might speculate on the nature of the fire type, e.g., smoldering or derived from nitrogen-rich fuel. However, we let the statistical technique define these types and so apply basic clustering techniques. We used nonnegative matrix factorization (NMF), but Mahalanobis clustering or other techniques seem to do equally well. NMF and  $k$ -means clustering are shown to be equivalent in cases corresponding to our work (Ding et al., 2005). A larger number of cluster classes will allow more ability to follow the EnR actually characteristic of the observation but at the cost of parsimony and sensitivity to instrumental error for the species or property. We used the R routine *nmf()* with  $k = 6$  components and the Lee estimation technique with singular-value initialization (Lee and Seung, 2001; Boutsidis and Gallopoulos, 2008). Use of the singular-value option for initialization proved satisfactory; it agreed well with the default method.

Since all fire tracers are correlated, such clustering characterizations are much better defined if based on a rough normalization to the fuel burned. We used a consensus variable, composed from all the defining tracers, to act as an agent for constructing ratios:

$$v_i = \text{mean}_j(y_{ij}). \quad (21)$$

This ratioing variable plays a role logically played by  $C_{\text{burn}} = (x_i - x_i^0)$ . Exact quantitative calibration of  $C_{\text{burn}}$  in parts per million is not required, just a relative scale is. We found it could be intuitively helpful to conceive of the ratioing variable in parts per million of carbon, just as with our later estimate of  $C_{\text{burn}}$ . To assign parts-per-million values, see the Supplement, “Note on an Early Approximate  $C_{\text{burn}}$ ”.

We end this section on methodology describing a separate strand of analysis. We sought timescales that could be inferred from the data, which could distinguish the relative age of burning emissions. At greater distances from the fire, there is both aerosol transformation and photochemical loss and production of species. Photochemical processing appeared easier to diagnose. We followed the ideas of Roberts et al. (1984), McKeen and Liu (1993), Parrish et al. (2007), and Warneke et al. (2013). The Parrish et al. (2007) presentation was most directly relevant. For considerations of these plume samples, a single origin strongly controlling mixing ratios made analysis simpler. Following Eq. (3) of Parrish et al. (2007) and using the symbols E and Y for the mixing ratios of ethEne, and ethYne, respectively,

$$\tau_{\text{age}}(\text{OH}) = -\frac{1}{k_E - k_Y} \left( \ln \frac{Y_Y}{Y_E} - \ln \frac{E_Y}{E_E} \right). \quad (22)$$

In view of this we constructed estimates for each instance  $i$  of  $\log_{10}((y_Y)_i/(y_E)_i) - \text{constant}$ . The constant can be estimated with similar results (a) so that the shortest times are about +15 min or (b) from the highest observed values of  $\log_{10}((y_Y)_i/(y_E)_i)$ . The values of longer times are determined by the assumed value of  $[\text{OH}]$ . The references cited describe the fact that most  $\tau_{\text{age}}(\text{OH})$  observations have a contribution from mixing as well as photochemistry, but this has little effect on the relative ages. In view of the uncertainty in the history of  $[\text{OH}]$  during transport, we simply graph the log of the ratios. Data analysis suggested that the assumed background mixing ratios of the species of ethyne and ethene were small. The Supplement provides some more details and one estimate of the associated times (“Note on Sensitivity to Number of Tracers Used”).

### 6.3 Summary of the MERET algorithm and notes

A summary of the MERET method as we currently propose it is shown in Fig. 8. It contains many steps, due to the need to disentangle background  $(C_{\text{burn}})_i$  effects from  $a_j$  effects related to instance-by-instance EnRs and the variation in  $\hat{a}_j$  by fire type.

1. Select a dataset of likeliest forest fire emission plumes, where  $\text{CH}_3\text{CN} > 0.125$  ppt (clear biomass-burning signal) and excluding urban influence  $(\text{CO} - \text{CO}^{\text{Env}})/(\text{CO}_2 - \text{CO}_2^{\text{Backg}}) > 33 \times 10^{-3}$ .
2. Select  $N_{\text{Tracer}} > 3$  fire tracers with estimable environmental background values of  $y_j^{\text{E}}$  and subtract from plume instances. Nearby values sufficiently distant from plumes provide a good guide unless the tracer has very strong nonfire sources (e.g.,  $\text{CH}_4$  in California valleys).  $y_{ij}^{\text{prenormalized}} \leftarrow (y_{ij}^{\text{measured}} - y_j^{\text{E}})$ .
3. *Normalize* the tracers above backgrounds:  $y_{ij} = y_{ij}^{\text{prenormalized}} / \text{mean}_i(y_{ij}^{\text{prenormalized}})$ .
4. Create values *ratioed* to a general fire-influence parameter:  $v_i = \text{mean}_j(y_{ij})$ . Create  $y_{ij}/v_i$ . Preliminary  $(C_{\text{burn}}^{\text{Approx}})_i$  may be estimated based on  $v_i$ , for reference.
5. Roughly cluster plumes into  $N_{\text{Types}}$  clusters using ratioed values of  $y_{ij}/v_i$  to estimate fire types corresponding to varying EnRs common to species  $j$ . The value of  $N_{\text{Types}}$  was observed to make little difference. We used  $N_{\text{Types}} = 6$ . Allow  $j$  to signify tracers within clusters.
6. Use mixed-effects regression to make estimates of intercepts and slopes  $\hat{y}_{ij}^0$  and  $\hat{a}_j$  using a mixed-effects regression like `main.lmer`, allowing random effects corresponding to species (or species and type of fire) and by instance. Regress  $y_{ij} = a_j x_i + c_i^0 + e_{ij}$ , and estimate the fitted values of  $\hat{y}_{ij}$ .

7. Prepare to estimate  $\hat{x}_{ij}^0$ . For numerical reasons, select an offset to apply to plumes that follows lower plume values, approximately 2 ppm less. Better discrimination makes for tighter estimates of  $\hat{x}_{ij}^0$  in the next step.
8. Calculate  $\hat{x}_{ij}^0 = (\hat{y}_{ij} - y_{ij}^0)/\hat{a}_j$  from the fitted  $\hat{y}_{ij}$  values: take  $\hat{x}_i^0 = \text{median}_j \hat{x}_{ij}^0$ . Medians are little affected by exact choices in item 7, but spreads of estimates are affected.
9. Estimate  $(C_{\text{burn}})_i = (x_i - \hat{x}_i^0)$ . The results for equivalent-background  $\hat{x}_i^0$  and  $C_{\text{burn}}$  are shown in Fig. 9 and are discussed more in Sect. 7. EnRs may now be calculated using Eq. (20). One may also use  $(C_{\text{burn}})_i$  recursively, returning to steps 4–9 until convergence. However, for our dataset this made an inconsequential difference.
10. Use  $(x_i - \hat{x}_{ij}^0)$  to estimate EnRs for any fire emission including tracers, using EnR for each  $i$  and  $j = (y_{ij}^{\text{measured}} - y_j^{\text{E}})/(x_i - \hat{x}_i^0)$ ; evaluate EnR to estimate ER and EF, considering possible transformation from the emission to measurement point.

More technical observations are these:

- a. For the use of an offset in calculations, we subtracted a baseline,  $C_{\text{baseline}}$ , a value determined as a constant for contiguous intervals, shown later in Sect. 7 and Fig. 9, and yielding a  $\sim 2$  ppm offset. We found that this minimized *skewness* and *variance* in the  $\hat{x}_{ij}^0$  estimates for each observation instance  $i$ . It is comforting that the effect of differing offsets on the values of the *median*,  $\hat{x}_i^0$ , is small,  $< 1$  ppm. (Add the offset back into the  $C_{\text{baseline}}$  when reporting  $\hat{x}_i^0$ .)
- b. Note that sharp positive and negative excursions of  $\hat{x}_i^0$  are seen near dramatic spikes in  $x_i$ . However,  $(x_i - \hat{x}_i^0)$  and consequently the EnRs are little affected. We can only speculate that small differences in the time averaging of  $\text{CO}_2$  and the tracers due to the instruments may explain these. Note also that the number of parameters  $N_{\text{Tracer}} \cdot N_{\text{Types}} + N_{\text{Instance}}$  for the mixed-effects regression remains  $\ll N_{\text{Tracer}} \cdot N_{\text{Instance}}$  so that the mixed-effects regression is very strongly determined.
- c. The number of classes allowed in step 5 matters little over two or three. Adding additional classes (clusters) tends to add only minor variations in the slopes  $\hat{a}_j$ . We are aware that overfitting effects can occur with many regression terms with positive and negative terms which mainly allow fitting of special cases. Here, harmful effects seen in overfitting of regression models are largely avoided by a requirement that the  $\hat{a}_j$  values be positive.

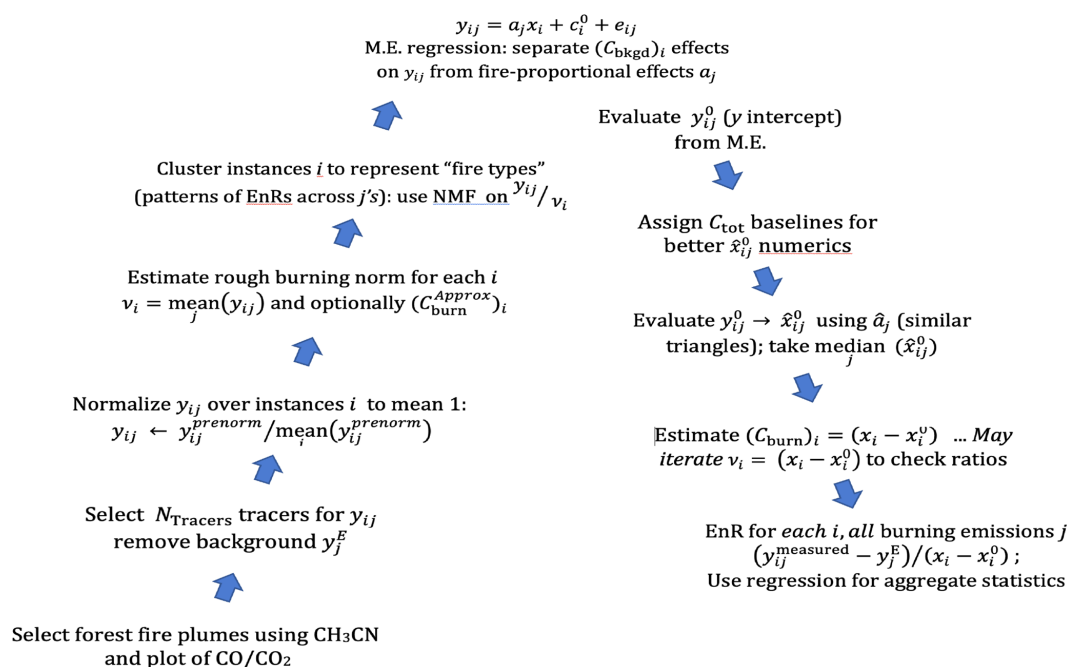


**Figure 8.** Summary of the MERET algorithm. See text for further detail.

- d. As noted, it is possible to use this method recursively, making presumably better classifications of fire types. In our experience, while it is possible to make convergent, recursive characterizations of the  $C_{\text{burn}}$  quantity, tighter clustering, and more precise mixed-model lmer() estimates, the quantities  $x_i^0$  and  $(x_i - x_i^0)$  were just significant enough to warrant such care. If we had fewer than eight tracers available, such recursion might be important. We will incrementally update documentation of the code (Chatfield, 2020). New applications of the code will suggest improvements.

Here we outline a check on the consistency of  $C_{\text{burn}}$  estimation. The results for  $C_{\text{burn}}$  and tracer EnRs suggested to us that one likely source of uncertainty is that  $C_{\text{burn}}$ ,  $\hat{x}_i^0$ , and the tracers may change very rapidly in comparison to our 1 min sampling intervals. Looking into this, we found that many of the  $C_{\text{burn}}$  estimates are of small magnitude; 12 of the 422 samples yielded  $C_{\text{burn}} < 1.5$  ppm. Even large jumps from sample to sample in estimated  $\hat{x}_i^0$  were not particularly associated with anomalous estimates of  $C_{\text{burn}}$ . The remaining, appealing possibility is occasional imprecise time alignment of all measurements, particularly of the  $\text{CO}_2$  measurements. Such imprecise alignment could happen at any stage, from sampling line delays to interpolation to 1 min time intervals. Such variations in  $\text{CO}_2$  would affect the  $\hat{x}_{ij}^0$  found for all tracers in a coordinated way, just as was observed. Note that estimates of  $C_{\text{burn}}$  were little affected, since significant  $\hat{x}_{ij}^0$  excursions were associated with large  $\text{CO}_2 + \text{CO}$  values. See Supplement, “Note on Examples of Enhancement Ratios”.

#### 6.4 Number of independent samples

A natural broader question is, how well do these mean EnRs for a species represent the EnRs that might be measured in a large suite of significant forest fires in the Western USA? Clearly, this question can only be asked in the context of the sample provided by the two campaigns. Instances when the aircraft continued to sample smoke for many minutes could contain several types of plumes, as we will see illustrated for the Rim Fire plume of August 2013. The use of 10 s averages (if available) would not provide 6 times as much information about fire plumes as 60 s averages over the same measurement run. We tried a simple, approximate quantification of “independent instances” available to us using a frequently used formulation by Trenberth (1984). This can also be seen as providing one answer to the question, how many effectively independent samples of  $C_{\text{burn}}$  are there contributing to a mean, standard deviation, etc., of  $C_{\text{burn}}$  or the emissions factors for species, e.g., the  $\text{CO}$  tracer? That could be useful if instruments appeared to give imprecise measurements that required averaging. Trenberth assessed the correlation of successive observations by estimating an autoregressive AR(1) (i.e., Markov chain) model for a random variable  $\xi_i$  with parameter  $\phi$  and random error  $\varepsilon_i$ , i.e., estimate of  $\xi_{i+1} = \phi \xi_i + \varepsilon_i$ . We applied this for  $\xi_i = x_i - x_i^0 (= C_{\text{burn}})$  and several fire tracers  $y_{ij}$ , like toluene. Most contiguous sampling periods suggested around 0.6; this suggested Trenberth’s “effective time between independent observations” as  $\approx (1 + \phi)/(1 - \phi)$ , about 4 min. For the DC-8, 4 min corresponds to about 15 km at lower-tropospheric airspeeds. The

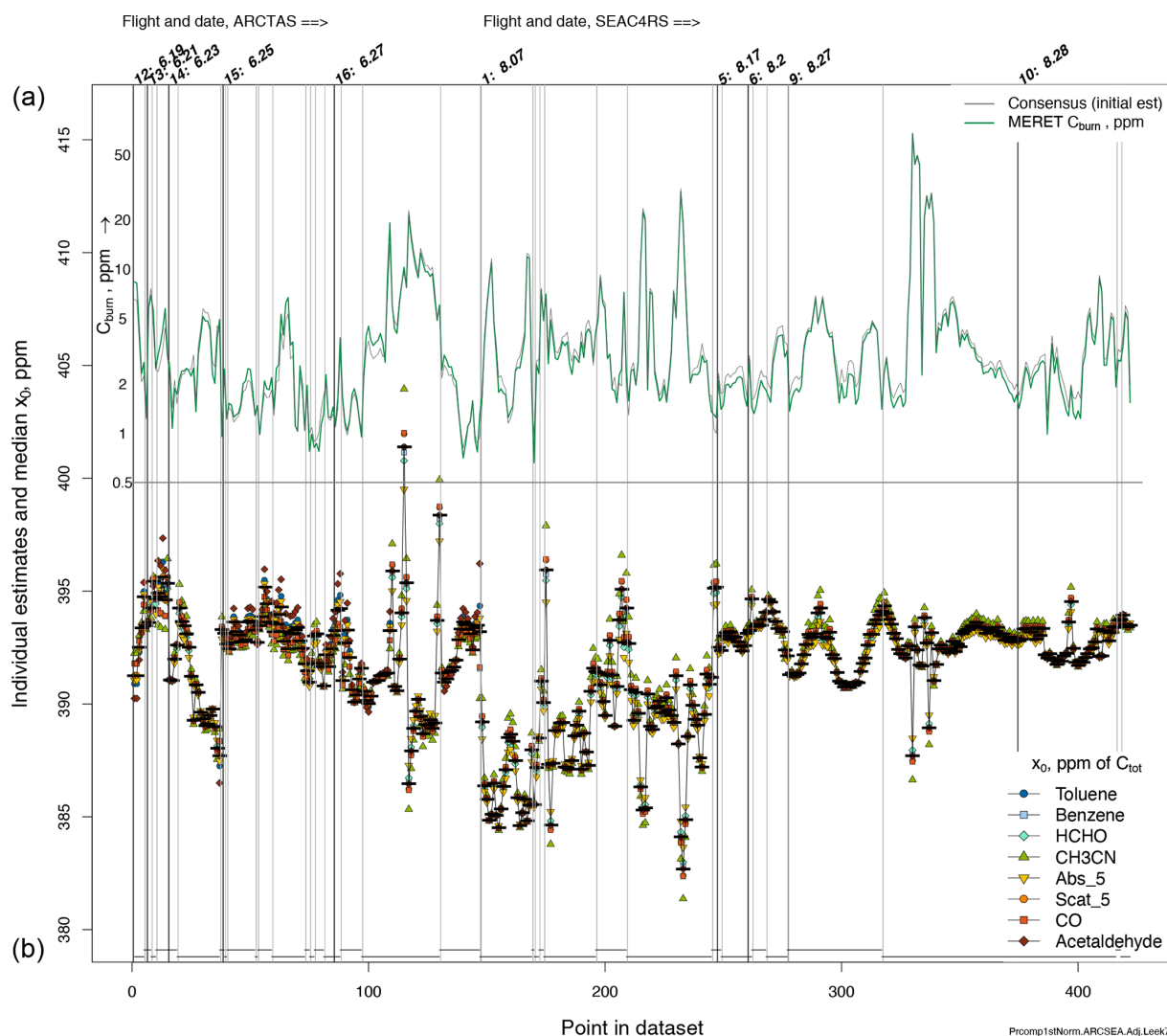


**Figure 9.** (b) Estimates of the 422 background  $\hat{x}_i^0 = \text{CO}_2 + \text{CO}$  concentrations implied based on the eight fire tracers indicated in the legend. Contributing individual estimates  $\hat{x}_{ij}^0$  are shown by overlapping colored points, with the median estimate  $\hat{x}_i^0$  indicated by a black bar. Usually the colored points overlap closely; this indicates strong agreement. (a) Estimates of  $C_{\text{burn}} = x_i - \hat{x}_i^0$  indicators of fuel carbon burned, in the thick green line. The preliminary estimate of  $C_{\text{burn}}$  based on the consensus of tracer deviations (without variable EnR estimates) is also shown in a thin line. A scale factor, maximizing overlap with the thick line, was necessarily estimated by regression. Flight days are indicated by the days marked on the top axes, and individual plumes, separated by nonplume concentrations of longer than 10 min, are shown as vertical separator lines. A set of horizontal lines at  $\sim 400$  ppm indicate selected intervals for optimizing numerics (see text, Sect. 6.3, item 7).

effect of this on the formal standard errors as described by a normal distribution was to increase them by a factor of  $\sim 2$ . Roughly similar effects are expected for the empirical descriptions of EnR variability described below. Undoubtedly, for plumes within minutes of the source, the number of degrees of freedom corresponds more closely to the number of 1 min observations, but the number of such samples is low.

Not surprisingly, *residuals* in regressions of CO against  $C_{\text{burn}}$  are very little correlated. We surmise that such low correlation gives confidence in the mathematical determination of the mean regression slope. However, it does not provide

help in answering the larger question, that of relevance in new situations. The sequential samples of plumes may have features like nonstationarity and selection bias; we hope that these ideas suggest more sophisticated analyses of relevance, left to future work.

## 7 Results – estimation of $\hat{x}_i^0$ and $C_{\text{burn}}$

The important results of the mixed model are the background  $\hat{x}_i^0$  and even more importantly the incremental carbon liberated to the atmosphere,  $C_{\text{burn}} = x_i - \hat{x}_i^0$ . The background es-

timates of  $\hat{x}_i^0$  for all samples and the contributing individual estimates  $\hat{x}_{ij}^0$  are shown in Fig. 9. The median  $\hat{x}_i^0$  is shown as a thin black line. The colored circles in the legend identify how the tracer species  $j$  contribute an individual  $\hat{x}_{ij}^0$  value, determining the median  $\hat{x}_i^0$ .

What are the uncertainties in the estimates we have made of  $\hat{x}_i^0$  and  $C_{\text{burn}}$ ? The uncertainty in estimated carbon burned ( $x_i - \hat{x}_i^0$ ) plays an important role in the ultimate estimates, the emission factors. In this section, we will confine our exposition to this uncertainty for now. The graphs of  $\hat{x}_i^0$  and ( $x_i - \hat{x}_i^0$ ) shown in Fig. 9 provide a practical understanding of the uncertainty. Note the continuity in  $\hat{x}_i^0$ ; this important observation is described below. Traditional estimation of uncertainties for ( $x_i - \hat{x}_i^0$ ) is complex due to the several steps involved and the use of median estimates. The advisability of using the median estimator and its statistical properties have long been recognized (Laplace, 1774; Lawrence, 2013). This variety of uncertainty estimation may be useful as MERET is refined. However, we expect that the study of uncertainty depends more on evaluating sources of true variability in the EnRs and also on the conservation of tracer concentrations from the flames to the sampling point than on the mathematics of median estimation. Consequently, the following paragraphs explore these questions related to the number and choice of tracers. We suggest that the typical strong overlap of the individual-tracer values may reflect the high precision of the observer's techniques!

How does the number of tracers affect results? What are the effects of using alternate or simpler sets of tracers? How many tracers are required for stable estimates? We began to address these questions by examining estimates made with fewer tracers in the intercept-determining set: the selection of the set of  $j$  values. The Supplement gives two examples of subsets ("Note on Sensitivity to Number of Tracers Used"). Here is a summary of that material. The two sets chosen are those that are the most unambiguous indicators of  $\hat{x}_{ij}^0$  based on their mutual agreement with  $\hat{x}_i^0$  from the full set of 10 tracers. They are Set 1 (CO, Scat\_5, and HCHO) and Set 2 (CO, Scat\_5, HCHO, acetaldehyde, and toluene). These are indicated by an examination of Fig. S2 in the Supplement. (Abs\_5 contributed  $\hat{x}_{ij}^0$ , which is the most deviating estimate from  $\hat{x}_{ij}^0$ .) Set 2 gave variations around of 0.02 ppm; the smaller set, Set 1, gave very similar variations except for the flights of 22 and 25 June, where many observation instances varied by around 0.1 ppm but with 11 points out of 422 differing by 0.3 ppm. This level of agreement surprised us. More significantly for our aims, the relative error in  $C_{\text{burn}}$  was only about 2 %. When sets containing the less correlated tracers were used, deviations ranged up to 0.2–0.4 ppm, which still appeared remarkably small.

Observation-to-observation consistency in  $\hat{x}_i^0$  estimates, seen for most plumes observed in Fig. 9, is the strongest argument for the precision of the  $C_{\text{burn}}$  estimates. Recall that our theory does not use sequential time information; thus, suc-

cessive estimates are essentially independent of each other. There is of course the dependency due to each observation's contribution to the estimate as one component of the *entire dataset*. This continuity is maintained even though the magnitudes of  $\text{CO}_2 + \text{CO}$  and estimated  $C_{\text{burn}}$  can change dramatically as the sampling aircraft enters and leaves each plume. Smooth excursions seen early in the flight marked 8.27 are explicable in terms of large changes in sampling altitude and location around the Rim Fire on that day. There are variations in  $\hat{x}_i^0$  from plume to plume and from day to day.

In contrast to this typical continuity of  $\hat{x}_i^0$  estimates, there are 15 to 20 brief and large excursions which deserve some attention. Of course, these may be disregarded in obtaining a general picture of EnRs. All the tracers suggest these excursions of the median, although there is a larger variation between the individual-tracer-based estimates  $\hat{x}_{ij}^0$ . These excursions are always associated with large changes in  $\text{CO}_2 + \text{CO}$  and  $C_{\text{burn}}$ , but often they occur 1 min later. We examined these excursions in detail. They do not seem to relate to changes in the EnRs'  $\hat{a}_j$  (as qualified by fire type) estimated simultaneously. The observations  $y_{ij}$  and the fitted  $\hat{y}_{ij}$  agree well, as do the nonexcursion points. Note however, that we may only use a single set of fire types, independent of  $j$ , to construct a set of  $\hat{a}_j$  values and  $\hat{y}_{ij}$  to make the  $\hat{x}_{ij}^0$  estimates.

The results for  $C_{\text{burn}}$  and tracer EnRs suggested to us that one likely source of uncertainty is that  $C_{\text{burn}}$ ,  $\hat{x}_i^0$ , and the tracers may change very rapidly in comparison to our 1 min sampling intervals. This would seem to be a concern since some  $C_{\text{burn}}$  estimates are of a small magnitude: 12 of the 422 samples yielded  $C_{\text{burn}} < 1.5$  ppm. However, large jumps from sample to sample in estimated  $\hat{x}_i^0$  were not particularly associated with anomalous estimates of  $C_{\text{burn}}$ . The remaining, appealing possibility is occasional imprecise time alignment of all measurements, particularly of the  $\text{CO}_2$  measurements. Such imprecise alignment could happen at any stage, from sampling line delays to interpolation to 1 min time intervals. Such variations in  $\text{CO}_2$  would affect the  $\hat{x}_{ij}^0$  found for all tracers in a coordinated way, just as was observed. Note that estimates of  $C_{\text{burn}}$  were little affected, since significant  $\hat{x}_{ij}^0$  excursions were associated with large  $\text{CO}_2 + \text{CO}$  values.

MERET should work better with more tracers, since more fire types may be revealed. However, additional classes (clusters) tend to add only minor variations in the slopes  $\hat{a}_j$ . Furthermore, harmful effects often seen in the overfitting of regression models should be minimized by a requirement that the  $\hat{a}_j$  values be positive. (Positive and negative regression coefficients that allow the fitting of just a few points cannot be added.)



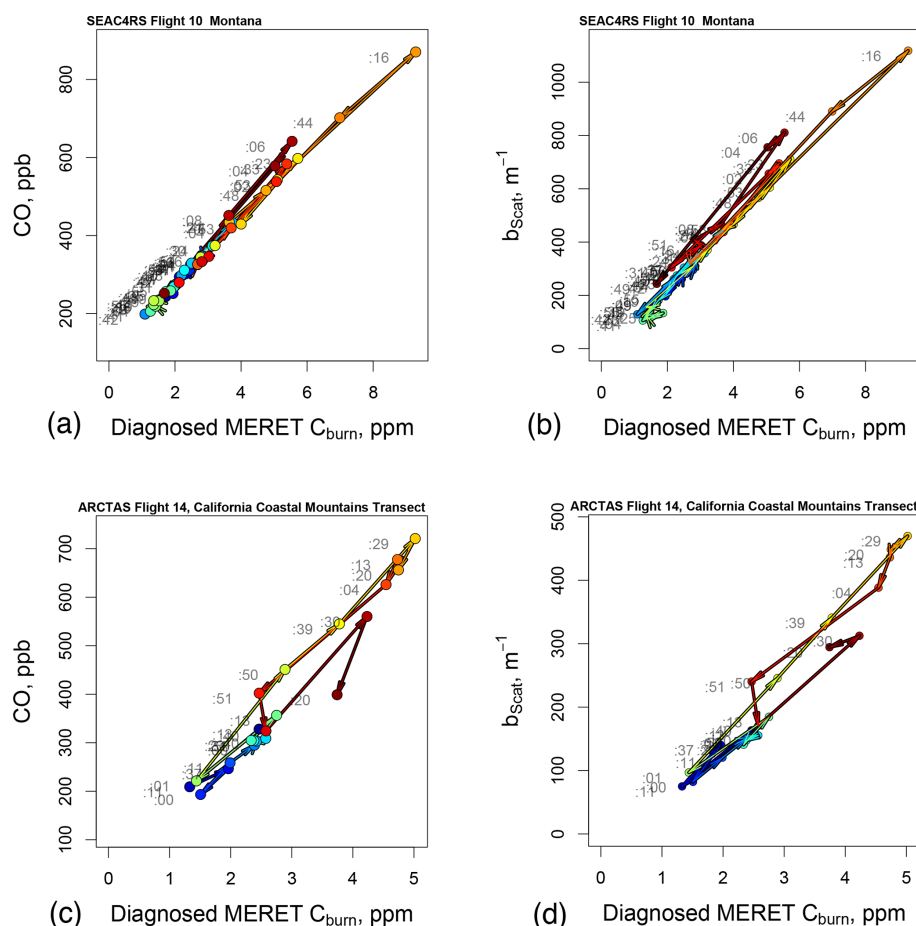


**Figure 10.** Analyzed relation of tracers to carbon burned using MERET for portions of SEAC4RS Flight 10 and ARCTAS Flight 14. Compare panels (a) through (d) with Fig. 4b, c, e, and f. Colors key the observations to times shown in the timelines in Fig. 4a and c. Light gray numerals give observation times in minutes.

## 8 Estimates of emission ratios – two MERET examples

### 8.1 MERET results for our two examples

The usefulness of our estimates of  $\hat{x}_i^0$  and  $C_{\text{burn}} = x_i - \hat{x}_i^0$  is seen in the MERET analysis (Fig. 10) of the two case studies analyzed above using the NEMR approach, with portions of flights 10 and 14 shown in Fig. 4. The tracers CO and  $b_{\text{scat}}$  appear much better correlated with the  $C_{\text{burn}}$  estimated from MERET, especially in Flight 14. The plots for both CO and scattering imply linear relationships with an implied intercept near 0; i.e., background values of  $y_i$  have been satisfactorily removed. Difficulties with a variable  $C_{\text{bgd}}$  appear to be resolved. However, the slopes of all the lines do not all agree. The Montana scatterplots (Fig. 4a) and (Fig. 4b) appear to suggest two slightly different linear features. The California transect scatterplots (Fig. 4c) and (Fig. 4d) show more separated linear features, though the slopes are parallel. We expect that these might correspond to varying fire types and perhaps varying MCEs, to be discussed in Chatfield and Andreae (2020), or to variations in background values of  $y_j^0$ ,

which are much harder to detect with either MERET or the NEMR approach. A combined approach, using MERET to locate regions of similar MCE, might be useful here. Also, note that the variation in slope is more evident for  $b_{\text{scat}}$  than CO, emphasizing the special role of CO as the single best fire tracer, closely followed by  $b_{\text{scat}}$ .

### 8.2 Table of several significant emissions

Table 3 provides a summary of the EnR relationships for some of the most significant gaseous emissions and particulate properties. In many cases, these EnRs can be converted to ERs and emission factors when the relationship of airborne  $C_{\text{burn}}$  to surface fuel consumed can be established. For the most highly reactive species, these EnRs will tend to be underestimates. An interpretive paper (Chatfield and Andreae, 2020) will give additional information on the photochemical age of the observation in many cases. Ozone and peroxy acetyl nitrate (PAN) are not emissions but produced in the plumes. Their relationships to fuel burned and their variations are nevertheless interesting. Descriptions of variation

**Table 3.** EnR estimates for fire emissions considered.

Fire emission	EnR estimate	Percentile 16	Percentile 84	Unit	Conversion factor to EF
CO	74	62	85	ppb ppm <sup>-1</sup>	1.17
CH <sub>4</sub>	8.6	2.3	13.0	ppb ppm <sup>-1</sup>	0.67
Ethyne	0.26	0.205	0.31	ppb ppm <sup>-1</sup>	1.08
Ethene	0.88	0.65	1.07	ppb ppm <sup>-1</sup>	1.17
Ethane	0.70	0.57	0.80	ppb ppm <sup>-1</sup>	1.25
Propene	0.056	0.005	0.100	ppb ppm <sup>-1</sup>	1.75
Propane	0.16	0.12	0.19	ppb ppm <sup>-1</sup>	1.83
n-Butane	0.028	0.019	0.037	ppb ppm <sup>-1</sup>	2.17
Benzene	0.094	0.073	0.134	ppb ppm <sup>-1</sup>	3.25
Toluene	0.054	0.023	0.067	ppb ppm <sup>-1</sup>	3.88
Methanol	2.1	1.7	3.1	ppb ppm <sup>-1</sup>	1.33
HCHO	1.15	0.81	1.62	ppb ppm <sup>-1</sup>	1.25
Acetaldehyde	0.56	0.24	0.71	ppb ppm <sup>-1</sup>	1.83
Acetone	0.74	0.54	1.14	ppb ppm <sup>-1</sup>	2.42
CH <sub>3</sub> CN	0.13	0.11	0.16	ppb ppm <sup>-1</sup>	1.25
NO <sub>x</sub> (as N)	0.051	0.024	0.131	ppb ppm <sup>-1</sup>	0.63
O <sub>3</sub>	14.8	8.5	25.1	ppb ppm <sup>-1</sup>	(2.0)
PAN	0.26	0.17	0.38	ppb ppm <sup>-1</sup>	(3.17)
Scat <sub>5</sub> , <i>b</i> <sub>Scat</sub>	79	50	100	m <sup>-1</sup> ppm <sup>-1</sup>	0.042
Abs <sub>5</sub> , <i>b</i> <sub>Abs</sub>	3.2	2.2	4.4	m <sup>-1</sup> ppm <sup>-1</sup>	0.042
Ammonium	0.32	0.19	0.47	μg m <sup>-3</sup> ppm <sup>-1</sup>	0.032
Nitrate	0.28	0.11	0.60	μg m <sup>-3</sup> ppm <sup>-1</sup>	0.107
Sulfate	0.156	0.063	0.290	μg m <sup>-3</sup> ppm <sup>-1</sup>	0.164

Notes: conversions assume a *C* to dry biomass ratio of 0.5. Conversions to micrograms per cubic meter assume a temperature of 25 °C and atmospheric pressure of 1013 hPa. O<sub>3</sub> and PAN are not directly produced by fires. HCHO is produced but often decreases rapidly. Under appropriate conditions indicated in Chatfield and Andreae (2020), the EnR estimates can be used as ERs. For tracers that are rapidly removed or transformed, these tend to be the higher values. Parentheses in the last column indicate that the entry is an emission relationship, not EF, as O<sub>3</sub> and PAN are not directly emitted.

are given as the 16th and 84th percentiles of all the estimates. These are similar to error estimates if nothing more is known about the origin and age of the particular samples, a matter more fully discussed in Chatfield and Andreae (2020). EnRs as they varied in time and in relationship to measures of photochemical processing are shown in the Supplement, “Note on Examples of Enhancement Ratios”.

## 9 Conclusions

A major problem with the estimation of fire enhancement ratios and emission factors is inherent in their character: flames promote mixing in their plumes. Total carbon liberated to the atmosphere (approximately  $C_{\text{burn}} = \text{CO}_2 + \text{CO}$ ) is mixed with background air at different points in the plume’s evolution, and removal of that mixing effect has been a difficulty. The NEMR technique often uses CO as a unique tracer, but the EnR of CO is variable, adding uncertainty to the estimation of the EFs. Given the variability of CO due to combustion efficiency (MCE) and environmental variabil-

ity, it has been emphasized that the NEMR technique can only be confidently applied in situations in which conditions affecting the ratio of CO to ( $\text{CO}_2 + \text{CO}$ ) can be well determined, ideally from source to sampling (Yokelson et al., 2013). The method also tends to emphasize the use of samples of CO and tracer collected over many minutes so that the regression method for EnRs of tracer relative to CO, defining  $a_{\text{CO}} \leftarrow (\text{fire-added } C_{\text{burn}})$ , becomes stable and a conversion to fuel carbon burned becomes possible.

We sought to decompose  $C_{\text{tot}}$  into  $C_{\text{bgd}}$  and  $C_{\text{burn}}$ . However, meteorology and mixing allow significant variations in  $C_{\text{bgd}}$  due to other powerful processes, e.g., CO<sub>2</sub> from respiration and photosynthesis in mixed-layer air. Once lofted,  $C_{\text{bgd}}$  varies little unless the plume enters layers of free tropospheric air from long-range transport with different  $C_{\text{bgd}}$  values, which further dilute the plume (Yokelson et al., 2013). We noted such problems using the NEMR method in analyzing a significant number of plumes for enhancement ratios studied in the Western USA during two campaigns, ARCTAS California and SEAC4RS, with 1 min samples totalling 422 in all.

The problem of deriving an accurate  $C_{\text{bgd}}$  is solved by noticing that there are two different kinds of information provided by multiple observational instances of a tracer and multiple tracers at a single instance. Information about the various EnRs and  $C_{\text{bgd}}$  values is mixed but not inextricably. There is a solution based on mixed-effects (also called random-effects) regression modeling. We propose a mixed-effects regression emission technique (MERET) to replace or at least to check on the NEMR approach, for which we used the R routine `lmer()`.

MERET is related to traditional entraining-plume models for parcels. We presented a synthesis describing multiple tracers from fire to sampling location. Sample calculations with the model suggest that it deals linearly with several varied histories for plume mixing. This motivates a regression equation for an equivalent-background  $x_i^0$  value for each observation that is related to entraining concentrations  $x^E(t)$  along the trajectory and shows coherent agreement for each tracer species (Fig. 9). The theory then allows this  $x_i^0$  to be used to define  $C_{\text{burn}}$  and thus to define the EnR for any appropriate fire-derived variable. This technique should allow EnRs in more variable, difficult situations and allows estimates of EnRs for individual samples.

EnRs are useful for the estimation of emission factors when the plume age is short compared to the transformation timescale of the measured fire tracer, and we provide an approximate diagnostic for this age for most samples. Formaldehyde, acetaldehyde, the alkenes, benzene,  $\text{NO}_x$ ,  $b_{\text{Scat}}$ , and  $b_{\text{Abs}}$  particularly require such attention.

Carbon monoxide is usually the best single tracer that correlates with fire emissions ( $C_{\text{burn}}$ ), supporting the use of the NEMR technique. Our analysis suggests other tracers had EnR variations that collectively helped to distinguish  $C_{\text{burn}}$  from CO in regression. The NEMR methodology depends on a full analysis of the history of CO influences on a sample to obtain a reliable MCE. MERET allows estimates of MCE as well as of  $C_{\text{burn}}$  for each sample. Thus it demarcates sampling periods with nearly homogeneous MCE. However, possible large variations in the entraining background of CO should still be considered carefully in dilute plumes with  $C_{\text{burn}} < 2$  ppm.

### Questions for future research

We conclude with some questions for future research; these also review the suggested conclusions of this paper and acknowledge the limitations of a single publication.

1. How well can the use of one or a few tracers, e.g., CO,  $b_{\text{Scat}}$ , and HCHO, actually constrain EnRs and EFs when only a few instruments may be used? How many variables need to be measured or how fresh should the plumes be to allow CO to be used both as a fire tracer and to allow useful estimates of MCE?

2. Can MERET be used to identify time periods of relatively homogeneous MCE, and can that MCE value be used with the NEMR to create suitable EnRs? Since the NEMR uses differences sample by sample (in time), no minimum value of another tracer needs to be estimated. (Consider that MERET does allow some evaluation of the minimum value estimate to be assessed and a better minimum assigned.)
3. Can MERET, the NEMR, and better near-fire nonplume sampling help us to prevent misattribution of fire emissions? These would include observations for fire intake air, air likely to be entrained in ascent, and air surrounding a plume and likely to be entrained as a plume spreads downwind. Can simulations of entraining plumes aid this effort?
4. What do fire types represent, and which species or properties tend to correlate in their EnRs (Chatfield and Andreae, 2020)?

**Data availability.** ARCTAS and SEAC4RS data are available for download from these permanent NASA data repositories: Arctic Research of the Composition of the Troposphere from Aircraft and Satellites (ARCTAS; <https://www-air.larc.nasa.gov/missions/arctas/arctas.html>) (Arctic Research of the Composition of the Troposphere from Aircraft and Satellites, 2020) and Studies of Emissions and Atmospheric Composition, Clouds and Climate Coupling by Regional Surveys (SEAC4RS; <https://www-air.larc.nasa.gov/missions/seac4rs/>) (Studies of Emissions and Atmospheric Composition, Clouds and Climate Coupling by Regional Surveys, 2020).

**Supplement.** The supplement related to this article is available online at: <https://doi.org/10.5194/amt-13-7069-2020-supplement>.

**Team list.** ARCTAS Science Team: James Crawford (NASA Langley Research Center), Henry Fuelberg (Florida State University), Chris Hostetler (NASA Langley Research Center), Daniel Jacob (Harvard University), Hal Maring (NASA Headquarters), Philip B. Russell (NASA Ames Research Center), Kent Shiffer (NASA Ames Research Center), Hanwant Singh (NASA Ames Research Center), Kathy Thompson (Science Systems and Applications, Inc.), Bruce E. Anderson (NASA Langley Research Center), Eric Apel (National Center for Atmospheric Research), Donald R. Blake (University of California, Irvine), William H. Brune (Pennsylvania State University), Christopher A. Cantrell (National Center for Atmospheric Research), Ronald C. Cohen (University of California, Berkeley), Jack Dibb (University of New Hampshire), Glenn S. Diskin (NASA Langley Research Center), Alan Fried (University of Colorado), Johnathan W. Hair (NASA Langley Research Center), L. Greg Huey (Georgia Tech), Jose-Luis Jimenez (CIRES, University of Colorado), Yutaka Kondo (University of Tokyo), Richard E. Shetter (University of North Dakota), Robert Talbot (University of New Hampshire), Stephanie A. Vay (NASA Langley Research Center), Rodney Weber (Georgia Tech), Andrew Weinheimer (Na-

tional Center for Atmospheric Research), Paul Wennberg (Caltech), Armin Wisthaler (Universität Innsbruck and Universitet i Oslo), John Barrick (NASA Langley Research Center), Anthony Bucholtz (Naval Research Laboratory), Antony Clarke (University of Hawaii), Lawrence C. Freudinger (NASA Armstrong Flight Center), Charles Gatebe (NASA Goddard Space Flight Center), Athanasios Nenes (Georgia Tech), James Podolske (NASA Ames Research Center), Jens Redemann (University of Oklahoma), Sebastian Schmidt (University of Colorado Boulder), Anthony Strawa (NASA Ames Research Center), Brian Cairns (NASA Goddard Institute for Space Studies), Richard Ferrare (NASA Langley Research Center), Samuel Oltmans (NOAA ESRL, University of Colorado Boulder), Glenn Shaw (University of Alaska Fairbanks), Anne M. Thompson (NASA Goddard Space Flight Center), Bob Curry (NASA Armstrong Flight Center), David Easmunt (NASA Goddard Space Flight Center), Michael S. Wusk (NASA Langley Research Center).

SEAC4RS Science Team: Hal Maring (NASA Headquarters), Ken Jucks (NASA Headquarters), Jassim Al-Saadi (NASA Headquarters), Richard Eckman (NASA Headquarters), Alex Pszenny (NASA Headquarters), Kent Shiffer (NASA Ames Research Center), Jhony Zavaleta (NASA Ames Research Center), Michael Craig (NASA Ames Research Center), David Jordan (NASA Ames Research Center), Quincy Allison (NASA Ames Research Center), Dan Chirica (NASA Ames Research Center), Susan Tolley (NASA Ames Research Center), Erin Czech (NASA Ames Research Center), Erin Justice (NASA Ames Research Center), Katja Drdla (NASA Ames Research Center), Brian Toon (University of Colorado), Eric Jensen (NASA Ames Research Center), Rich Ferrare (NASA Langley Research Center), David Diner (NASA Jet Propulsion Laboratory), Anthony Bucholtz (Naval Research Laboratory), Lance Christensen (NASA Jet Propulsion Laboratory), Matt McGill (NASA Goddard Space Flight Center), Steve Platnick (NASA Goddard Space Flight Center), Brian Cairns (NASA Goddard Space Flight Center), Jim Anderson (Harvard University), Rushan Gao (NOAA ESRL), Bob Herman (NASA Jet Propulsion Laboratory), MJ Mahoney (NASA Jet Propulsion Laboratory), Rushan Gao (NOAA ESRL), Steve Wofsy (Harvard University), Sebastian Schmidt (University of Colorado), Elliot Atlas (University of Miami), Paul Bui (NASA Ames Research Center), Hanwant Singh (NASA Ames Research Center), Jack Dibb (University of New Hampshire), Phillip Russell (NASA Ames Research Center), Jose-Luis Jimenez (University of Colorado), Charles Brock (NOAA ESRL), Simone Tanelli (NASA Jet Propulsion Laboratory), Andreas Beyersdorf (NASA Langley Research Center), Anthony Bucholtz (Naval Research Laboratory), Samuel Hall (National Center for Atmospheric Research), Paul Wennberg (Caltech), Thomas Ryerson (NOAA ESRL), Glenn Diskin (NASA Langley Research Center), Armin Sorooshian (University of Arizona), Alan Fried (National Center for Atmospheric Research), John Hair (NASA Langley Research Center), Glenn Diskin (NASA Langley Research Center), Greg Huey (Georgia Tech), Rushan Gao (NOAA ESRL), Thomas Hanisco (NASA Goddard Space Flight Center), Bruce Anderson (NASA Langley Research Center), Paul Bui (NASA Ames Research Center), Karl Froyd (NOAA ESRL), Greg Huey (Georgia Tech), Armin Wisthaler (Universität Innsbruck), Jack Dibb (University of New Hampshire), Paul Lawson (SPEC Incorporated), Sebastian Schmidt (University of Colorado), Ronald Cohen (University of California, Berkeley), Donald Blake (University of Cali-

fornia, Irvine), Joshua Schwarz (NOAA ESRL), J. Vanderlei Martins (University of Maryland, Baltimore County), Lenny Pfister (NASA Ames Research Center), Henry Fuelberg (NASA Langley Research Center), Rennie Selkirk (Universities Space Research Association), Daniel Jacob (Harvard University), Arlindo Da Silva (NASA Goddard Space Flight Center), Paul Konopka (Georgia Tech), Ed Hyer (Naval Research Laboratory), Greg Charmichael (University of Iowa), Jennifer Olson (NASA Langley Research Center), Louisa Emmons (National Center for Atmospheric Research), Gao Chen (NASA Langley Research Center), Chip Trepte (NASA Langley Research Center), Jay Mace (University of Utah), Pat Minnis (NASA Langley Research Center), Eric Ray (NOAA ESRL), Karen Rosenlof (NOAA ESRL), Daniel Jacob (Harvard University), Robert Yokelson (University of Montana), Jeffery Reid (Naval Research Laboratory), Jens Redemann (NASA Ames Research Center), David Starr (NASA Goddard Space Flight Center), Johnny Luo (City College of New York), Jay Mace (University of Utah), Laura Pan (National Center for Atmospheric Research), David Starr (NASA Goddard Space Flight Center), Jay Mace (University of Utah), Johnny Luo (City College of New York), James Crawford (NASA Langley Research Center), Frank Culter (NASA Armstrong Flight Center), Patrick Lloyd (NASA Armstrong Flight Center), Rick Shetter (National Suborbital Education and Research Center), Adam Webster (National Suborbital Education and Research Center), Eric Buzay (National Suborbital Education and Research Center), David VanGilst (National Suborbital Education and Research Center), Jane Peterson (National Suborbital Education and Research Center), Tim Moes (NASA Armstrong Flight Center), Chris Miller (NASA Armstrong Flight Center), Mike Kapitzke (NASA Armstrong Flight Center), Denis Steele (NASA Armstrong Flight Center), Stuart Broce (NASA Armstrong Flight Center), Jan Nystrom (NASA Armstrong Flight Center), Kevin Kraft (NASA Armstrong Flight Center).

Some of the team have changed affiliations since their work was documented. Two members of NASA's Earth Science Project Office (ESPO) may direct you on how to make enquiries regarding either team; contact [marilyn.vasques@nasa.gov](mailto:marilyn.vasques@nasa.gov) or [bernadette.luna@nasa.gov](mailto:bernadette.luna@nasa.gov). Also, one of the leaders at NASA Headquarters has some knowledge of both teams' members; contact [barry.lefer@nasa.gov](mailto:barry.lefer@nasa.gov).

**Author contributions.** MOA contributed motivating ideas and an approach following on from Yokelson et al. (2013). RBC brought data into a suitable format and evaluated the suitability of tracers. He contributed the theory of parallel plume rise expressions for fire tracers and the mixed-effects modeling approach. RBC wrote the publication with considerable contributions from MOA. The science teams mentioned contributed excellent observations, including many that were examined but not directly used, and also useful analysis and support.

**Competing interests.** The authors declare that they have no conflict of interest.

**Acknowledgements.** Particular acknowledgment goes to the instrumental groups in Table 1 and Sect. 4 and the many contributing

efforts of the ARCTAS and SEAC4RS science teams and staff. The effort grew out of research funded by California Air Resources Board and San Joaquin Valley air regional authority, where difficulties with previous methodology became apparent. We appreciate reviews by Sherry Palaicos, Michal Segal-Rozenhaimer, Emma Yates, and especially Ralf Koppmann. Robert F. Esswein helped with certain data reformatting. We acknowledge the great value of the R programming language and the lme4 and NMF packages.

This research has been partially supported by the US NASA Earth Science Research Program research grants 13-ACCDAM13-0110 and ACPMAP14-0095 and by Earth Science salary support in association with more recent fire studies. Meinrat O. Andreae acknowledges extensive support from the German Max Planck Society and facilitation of recent research by the Scripps Institute of Oceanography.

**Financial support.** This research has been supported by the US NASA Earth Science Research Program research (grant nos. 13-ACCDAM13-0110 and ACPMAP14-0095), Earth Science salary support in association with more recent fire studies, and the German Max Planck Society.

The article processing charges for this open-access publication were covered by the Max Planck Society.

**Review statement.** This paper was edited by Eric C. Apel and reviewed by two anonymous referees.

## References

- Akagi, S. K., Yokelson, R. J., Wiedinmyer, C., Alvarado, M. J., Reid, J. S., Karl, T., Crounse, J. D., and Wennberg, P. O.: Emission factors for open and domestic biomass burning for use in atmospheric models, *Atmos. Chem. Phys.*, 11, 4039–4072, <https://doi.org/10.5194/acp-11-4039-2011>, 2011.
- Akagi, S. K., Craven, J. S., Taylor, J. W., McMeeking, G. R., Yokelson, R. J., Burling, I. R., Urbanski, S. P., Wold, C. E., Seinfeld, J. H., Coe, H., Alvarado, M. J., and Weise, D. R.: Evolution of trace gases and particles emitted by a chaparral fire in California, *Atmos. Chem. Phys.*, 12, 1397–1421, <https://doi.org/10.5194/acp-12-1397-2012>, 2012.
- Akagi, S. K., Yokelson, R. J., Burling, I. R., Meinardi, S., Simpson, I., Blake, D. R., McMeeking, G. R., Sullivan, A., Lee, T., Kreidenweis, S., Urbanski, S., Reardon, J., Griffith, D. W. T., Johnson, T. J., and Weise, D. R.: Measurements of reactive trace gases and variable O<sub>3</sub> formation rates in some South Carolina biomass burning plumes, *Atmos. Chem. Phys.*, 13, 1141–1165, <https://doi.org/10.5194/acp-13-1141-2013>, 2013.
- Alvarado, M. J. and Prinn, R. G.: Formation of ozone and growth of aerosols in young smoke plumes from biomass burning: 1. Lagrangian parcel studies, *J. Geophys. Res.-Atmos.*, 114, D09306, <https://doi.org/10.1029/2008jd011144>, 2009.
- Alvarado, M. J., Wang, C., and Prinn, R. G.: Formation of ozone and growth of aerosols in young smoke plumes from biomass burning: 2. Three-dimensional Eulerian studies, *J. Geophys. Res.-Atmos.*, 114, D011186, <https://doi.org/10.1029/2008jd011186>, 2009.
- Alvarado, M. J., Logan, J. A., Mao, J., Apel, E., Riemer, D., Blake, D., Cohen, R. C., Min, K.-E., Perring, A. E., Browne, E. C., Wooldridge, P. J., Diskin, G. S., Sachse, G. W., Fuelberg, H., Sessions, W. R., Harrigan, D. L., Huey, G., Liao, J., Case-Hanks, A., Jimenez, J. L., Cubison, M. J., Vay, S. A., Weinheimer, A. J., Knapp, D. J., Montzka, D. D., Flocke, F. M., Pollack, I. B., Wennberg, P. O., Kurten, A., Crounse, J., Clair, J. M. St., Wisthaler, A., Mikoviny, T., Yantosca, R. M., Carouge, C. C., and Le Sager, P.: Nitrogen oxides and PAN in plumes from boreal fires during ARCTAS-B and their impact on ozone: an integrated analysis of aircraft and satellite observations, *Atmos. Chem. Phys.*, 10, 9739–9760, <https://doi.org/10.5194/acp-10-9739-2010>, 2010.
- Andreae, M. O.: Emission of trace gases and aerosols from biomass burning – an updated assessment, *Atmos. Chem. Phys.*, 19, 8523–8546, <https://doi.org/10.5194/acp-19-8523-2019>, 2019.
- Andreae, M. O. and Merlet, P.: Emission of trace gases and aerosols from biomass burning, *Global Biogeochem. Cy.*, 15, 955–966, <https://doi.org/10.1029/2000GB001382>, 2001.
- Andreae, M. O., Browell, E. V., Garstang, M., Gregory, G. L., Harriss, R. C., Hill, G. F., Jacob, D. J., Pereira, M. C., Sachse, G. W., Setzer, A. W., Silva Dias, P. L., Talbot, R. W., Torres, A. L., and Wofsy, S. C.: Biomass burning emissions and associated haze layers over Amazonia, *J. Geophys. Res.*, 93, 1509–1527, 1988.
- Arctic Research of the Composition of the Troposphere from Aircraft and Satellites (ARCTAS): Data Archive: ARCTAS, NASA, available at: <https://www-air.larc.nasa.gov/missions/arctas/arctas.html>, last access: 12 August 2020.
- Barry, R. G. and Chorley, R. J.: *Atmosphere, Weather and Climate*, 7th edn., Routledge, London, UK, 1998.
- Bates, D., Maechler, M., Bolker, B., and Walker, S.: lme4: Linear mixed-effects models using Eigen and S4. R package version 1.1-7, available at: <http://CRAN.R-project.org/package=lme4> (last access: 4 August 2020), 2014.
- Baylon, P., Jaffe, D. A., Wigder, N. L., Gao, H., and Hee, J.: Ozone enhancement in western US wildfire plumes at the Mt. Bachelor Observatory: The role of NO<sub>x</sub>, *Atmos. Environ.*, 109, 297–304, <https://doi.org/10.1016/j.atmosenv.2014.09.013>, 2015.
- Boutsidis, C. and Gallopoulos, E.: SVD based initialization: A head start for nonnegative matrix factorization, *Pattern Recogn.*, 41, 1350–1362, <https://doi.org/10.1016/j.patcog.2007.09.010>, 2008.
- Chatfield, R. B.: package Estim.ARC.SEAC.ERs, available at: <https://github.com/RobertBChatfield/FireEmissionsEstimate/>, last access: 6 August 2020.
- Chatfield, R. B. and Andreae, M. O.: Emissions relationships among western forest fire plumes: II. Plume typing for sources of ozone and aerosol absorption, in preparation, 2020.
- Crutzen, P. J. and Andreae, M. O.: Biomass Burning in the Tropics: Impact on Atmospheric Chemistry and Biogeochemical Cycles, *Science*, 250, 1669–1678, <https://doi.org/10.1126/science.250.4988.1669>, 1990.
- Crutzen, P. J., Heidt, L. E., Krasnec, J. P., Pollock, W. H., and Seiler, W.: Biomass burning as a source of atmospheric gases CO, H<sub>2</sub>, N<sub>2</sub>O, NO, CH<sub>3</sub>Cl and COS, *Nature*, 282, 253–256, 1979.
- Ding, C., He, X., and Simon, H. D.: On the Equivalence of Non-negative Matrix Factorization and Spectral Clustering, *Pro-*

- ceedings of the 2005 SIAM International Conference on Data Mining, 21–23 April 2005, Newport Beach, CA, USA, <https://doi.org/10.1137/1.9781611972757.70>, 2005.
- Fried, A., Walega, J. G., Olson, J. R., Crawford, J. H., Chen, G., Weibring, P., Richter, D., Roller, C., Tittel, F. K., Heikes, B. G., Snow, J. A., Shen, H., O'Sullivan, D. W., Porter, M., Fuelberg, H., Halland, J., and Millet, D.: Formaldehyde Over North America and the North Atlantic During the Summer 2004 INTEX Campaign: Methods, Observed Distributions, and Measurement-Model Comparisons, *J. Geophys. Res.*, 113, D10302, <https://doi.org/10.1029/2007JD009185>, 2008.
- Galanter, M., Levy II, H., and Carmichael, G. R.: Impacts of biomass burning on tropospheric CO, NO<sub>x</sub>, and O<sub>3</sub>, *J. Geophys. Res.*, 105, 6633–6653, <https://doi.org/10.1029/1999JD901113>, 2000.
- Gaujoux, R.: An Introduction to NMF package, available at: <https://cran.r-project.org/web/packages/NMF/vignettes/NMF-vignette.pdf> (last access: 6 August 2020), 2014.
- Gaujoux, R. and Seoighe, C.: A flexible R package for nonnegative matrix factorization, *BMC Bioinformatics*, 11.1, p. 367, <https://doi.org/10.1186/1471-2105-11-367>, 2010.
- Greenberg J. P., Zimmerman P. R., Heidt L., and Pollock W.: Hydrocarbon and carbon monoxide emissions from biomass burning in Brazil, *J. Geophys. Res.*, 89, 1350–1354, 1984.
- Guyon, P., Frank, G. P., Welling, M., Chand, D., Artaxo, P., Rizzo, L., Nishioka, G., Kolle, O., Fritsch, H., Silva Dias, M. A. F., Gatti, L. V., Cordova, A. M., and Andreae, M. O.: Airborne measurements of trace gas and aerosol particle emissions from biomass burning in Amazonia, *Atmos. Chem. Phys.*, 5, 2989–3002, <https://doi.org/10.5194/acp-5-2989-2005>, 2005.
- Hanna, S. R., Briggs, G. A., and Hosker, R. P.: Handbook on Atmospheric Dispersion, Prepared for the US Department of Energy, Technical Information Center, US Department of Energy (DOE/TIC-11223), Oak Ridge, Tennessee, USA, 1982.
- Hobbs, P. V., Sinha, P., Yokelson, R. J., Christian, T. J., Blake, D. R., Gao, S., Kirchstetter, T. W., Novakov, T., and Pilewskie, P.: Evolution of gases and particles from a savanna fire in South Africa, *J. Geophys. Res.*, 108, 8485, <https://doi.org/10.1029/2002JD002352>, 2003.
- Hornbrook, R. S., Blake, D. R., Diskin, G. S., Fried, A., Fuelberg, H. E., Meinardi, S., Mikoviny, T., Richter, D., Sachse, G. W., Vay, S. A., Walega, J., Weibring, P., Weinheimer, A. J., Wiedinmyer, C., Wisthaler, A., Hills, A., Rierner, D. D., and Apel, E. C.: Observations of nonmethane organic compounds during ARCTAS – Part 1: Biomass burning emissions and plume enhancements, *Atmos. Chem. Phys.*, 11, 11103–11130, <https://doi.org/10.5194/acp-11-11103-2011>, 2011.
- Jacob, D. J., Crawford, J. H., Maring, H., Clarke, A. D., Dibb, J. E., Emmons, L. K., Ferrare, R. A., Hostetler, C. A., Russell, P. B., Singh, H. B., Thompson, A. M., Shaw, G. E., McCauley, E., Pederson, J. R., and Fisher, J. A.: The Arctic Research of the Composition of the Troposphere from Aircraft and Satellites (ARCTAS) mission: design, execution, and first results, *Atmos. Chem. Phys.*, 10, 5191–5212, <https://doi.org/10.5194/acp-10-5191-2010>, 2010.
- Jaffe, D. and Wigder, N.: Ozone production from wildfires: a critical review, *Atmos. Environ.*, 51, 1–10, <https://doi.org/10.1016/j.atmosenv.2011.11.063>, 2012.
- Koppmann, R., Khedim, A., Rudolph, J., Poppe, D., Andreae, M. O., Helas, G., Welling, M., and Zenker, T.: Emissions of organic trace gases from savanna fires in southern Africa during the 1992 Southern African Fire Atmosphere Research Initiative and their impact on the formation of tropospheric ozone, *J. Geophys. Res.*, 102, 18879–18888, 1997.
- Laplace, P. S.: Mémoire sur la Probabilité des Causes par les Événements, *Mémoires de Mathématique et de Physique, Présentés à l'Académie Royale des Sciences, Par Divers Savans & Lûs Dans ses Assemblées*, 6, 621–656, 1774.
- Lareau, N. P. and Clements, C. B.: The Mean and Turbulent Properties of a Wildfire Convective Plume, *J. Appl. Meteorol. Clim.*, 56, 2289–2299, <https://doi.org/10.1175/JAMC-D-16-0384.1>, 2017.
- Lawrence, J.: Distribution of the Median in Samples from the Laplace Distribution, *Open Journal of Statistics*, 3, 422–426, <https://doi.org/10.4236/ojs.2013.36050>, 2013.
- Lee, D. D. and Seung, H. S.: Algorithms for Non-negative Matrix Factorization, in: *Advances in Neural Information Processing Systems*, Vol. 13, edited by: Leen, T., Dietterich, T., and Tresp, V., available at: <https://proceedings.neurips.cc/paper/2000/file/f9d1152547c0bde01830b7e8bd60024c-Paper.pdf> (last access: 12 August 2020), MIT Press, Cambridge, Massachusetts, USA, 556–562, 2001.
- Lefer, B. L., Talbot, R. W., Harriss, R. C., Bradshaw, J. D., Sandholm, S. T., Olson, J. O., Sachse, G. W., Collins, J., Shipman, M. A., Blake, D. R., Klemm, K. I., Gorzelska, K., and Barriack, J.: Enhancement of acidic gases in biomass burning impacted air masses over Canada, *J. Geophys. Res.*, 99, 1721–1737, <https://doi.org/10.1029/93JD02091>, 1994.
- Leighton, P.: *The Photochemistry of Air Pollution*, Academic Press, New York, USA, 1961.
- Liu, X., Huey, L. G., Yokelson, R. J., Selimovic, V., Simpson, I. J., Müller, M., Jimenez, J. L., Campuzano-Jost, P., Beyersdorf, A. J., Blake, D. R., Butterfield, Z., Choi, Y., Crounse, J. D., Day, D. A., Diskin, G. S., Dubey, M. K., Fortner, E., Hanisco, T. F., Hu, W., King, L. E., Kleinman, L., Meinardi, S., Mikoviny, T., Onasch, T. B., Palm, B. B., Peischl, J., Pollack, I. B., Ryerson, T. B., Sachse, G. W., Sedlacek, A. J., Shilling, J. E., Springston, S., St. Clair, J. M., Tanner, D. J., Teng, A. P., Wennberg, P. O., Wisthaler, A., and Wolfe, G. M.: Airborne measurements of western U.S. wildfire emissions: comparison with prescribed burning and air quality implications, *J. Geophys. Res.-Atmos.*, 122, 6108–6129, <https://doi.org/10.1002/2016JD026315>, 2017.
- McKeen, S. A. and Liu, S. C.: Hydrocarbon ratios and photochemical history of air masses, *Geophys. Res. Lett.*, 21, 2319–2413, <https://doi.org/10.1029/93GL02527>, 1993.
- McKeen, S. A., Liu, S. C., Hsie, E.-Y., Lin, X., Bradshaw, J. D., Smyth, S., Gregory, G. L., and Blake, D. R.: Hydrocarbon ratios during PEM-WEST A: A model perspective, *J. Geophys. Res.*, 101, 2087–2109, <https://doi.org/10.1029/95JD02733>, 1996.
- Morton, B. R., Taylor, G. I., and Turner, J. S.: Turbulent gravitational convection from maintained and instantaneous sources, *P. Roy. Soc. Lond.*, A234, 1–23, 1956.
- National Research Council: *Estimating Mortality Risk Reduction and Economic Benefits from Controlling Ozone Air Pollution*. National Academies Press, Washington, D.C., USA, 2008.
- Parrish, D. D., Stohl, A., Forster, C., Atlas, E. L., Blake, D. R., Goldan, P. D., Kuster, W. C., and de Gouw, J. A.: Effects of mixing on evolution of hydrocarbon ra-



- tios in the troposphere, *J. Geophys. Res.*, 112, D10S34, <https://doi.org/10.1029/2006JD007583>, 2007.
- Pfister, G. G., Avise, J., Wiedinmyer, C., Edwards, D. P., Emmons, L. K., Diskin, G. D., Podolske, J., and Wisthaler, A.: CO source contribution analysis for California during ARCTAS-CARB, *Atmos. Chem. Phys.*, 11, 7515–7532, <https://doi.org/10.5194/acp-11-7515-2011>, 2011.
- Pinheiro, J. C. and Bates, D. M.: *Mixed-Effects Models in S and S-PLUS*, Springer, New York, USA, 2000.
- Poppe, D., Koppmann, R., and Rudolph, J.: Ozone formation in biomass burning plumes: Influence of atmospheric dilution, *Geophys. Res. Lett.*, 25, 3823–3826, 1998.
- Reid, J. S., Koppmann, R., Eck, T. F., and Eleuterio, D. P.: A review of biomass burning emissions part II: intensive physical properties of biomass burning particles, *Atmos. Chem. Phys.*, 5, 799–825, <https://doi.org/10.5194/acp-5-799-2005>, 2005.
- Roberts, J. M., Fehsenfeld, F. C., Liu, S. C., Bollinger, M. J., Hahn, C., Albritton, D. L., and Sievers, R. E.: Measurements of aromatic hydrocarbon ratios and  $\text{NO}_x$  concentrations in the rural troposphere: Estimates of air mass photochemical age and  $\text{NO}_x$  removal rate, *Atmos. Environ.*, 18, 2421–2432, 1984.
- Ryerson, T. B., Williams, E. J., and Fehsenfeld, F. C.: An efficient photolysis system for fast-response  $\text{NO}_2$  measurements, *J. Geophys. Res.-Atmos.*, 21, 26447–2646, <https://doi.org/10.1029/2000JD900389>, 2000.
- Seinfeld, J. H. and Pandis, S. N.: *Atmospheric Chemistry and Physics: From Air Pollution to Climate Change*, 3rd edn., Wiley, Hoboken, New Jersey, USA, 2016.
- Simpson, I. J., Akagi, S. K., Barletta, B., Blake, N. J., Choi, Y., Diskin, G. S., Fried, A., Fuelberg, H. E., Meinardi, S., Rowland, F. S., Vay, S. A., Weinheimer, A. J., Wennberg, P. O., Wiebring, P., Wisthaler, A., Yang, M., Yokelson, R. J., and Blake, D. R.: Boreal forest fire emissions in fresh Canadian smoke plumes:  $\text{C}_1$ – $\text{C}_{10}$  volatile organic compounds (VOCs),  $\text{CO}_2$ ,  $\text{CO}$ ,  $\text{NO}_2$ ,  $\text{NO}$ ,  $\text{HCN}$  and  $\text{CH}_3\text{CN}$ , *Atmos. Chem. Phys.*, 11, 6445–6463, <https://doi.org/10.5194/acp-11-6445-2011>, 2011.
- Singh, H. B. and the ARCTAS Science Team: Pollution influences on atmospheric composition and chemistry at high northern latitudes: Boreal and California forest fire emissions, *Atmos. Environ.*, 44, 4553–4564, 2010.
- Singh, H. B., Cai, C., Kadowela, A., Weinheimer, A., and Wisthaler, A.: Interactions of fire emissions and urban pollution over California: Ozone formation and air quality simulations, *Atmos. Environ.*, 56, 45–51, 2012.
- Squires, P. and Turner, J. S.: An entraining jet model for cumulonimbus updraughts, *Tellus A*, 14, 422–434, 1962.
- Studies of Emissions and Atmospheric Composition, Clouds and Climate Coupling by Regional Surveys (SEAC4RS): Data Archive: SEAC4RS, NASA, available at: <https://www-air.larc.nasa.gov/missions/seac4rs/>, last access: 12 August 2020.
- Toon, O. B., Maring, H., Dibb, J., Ferrare, R., Jacob, D. J., Jensen, E. J., Luo, Z. J., Mace, G. G., Pan, L. L., Pfister, L., Rosenlof, K. H., Redemann, J., Reid, J. S., Singh, H. B., Thompson, A. M., Yokelson, R., Minnis, P., Chen, G., Jucks, K. W., and Pszenny A.: Planning, implementation and scientific goals of the Studies of Emissions and Atmospheric Composition, Clouds and Climate Coupling by Regional Surveys (SEAC4RS) field mission, *J. Geophys. Res.-Atmos.*, 121, 4967–5009, <https://doi.org/10.1002/2015JD024297>, 2016.
- Trenberth, K.: Some effects of finite sample size and persistence on meteorological statistics. Part I: Autocorrelations, *Mon. Weather Rev.*, 112, 2359–2368, 1984.
- Trentmann, J., Andreae, M. O., Graf, H.-F., Hobbs, P. V., Ottmar, R. D., and Trautmann, T.: Simulation of a biomass burning plume: Comparison of model results with observations, *J. Geophys. Res.*, 107, 4013, <https://doi.org/10.1029/2001JD000410>, 2002.
- U.S. EPA: U.S. Environmental Protection Agency 2002 National Emissions Inventory, available at: [ftp://newftp.epa.gov/air/nei/nei\\_criteria\\_summaries/2002summaryfiles/](ftp://newftp.epa.gov/air/nei/nei_criteria_summaries/2002summaryfiles/) (last access: 6 August 2020), 2006.
- van Leeuwen, T. T. and van der Werf, G. R.: Spatial and temporal variability in the ratio of trace gases emitted from biomass burning, *Atmos. Chem. Phys.*, 11, 3611–3629, <https://doi.org/10.5194/acp-11-3611-2011>, 2011.
- Vay, S. A., Choi, Y., Vadrevu, K. P., Blake, D. R., Tyler, S. C., Wisthaler, A., Hecobian, A., Kondo, Y., Diskin, G. S., Sachse, G. W., Woo, J.-H., Weinheimer, A. J., Burkhardt, J. F., Stohl, A., and Wennberg, P. O.: Patterns of  $\text{CO}_2$  and radiocarbon across high northern latitudes during IPY 2008, *J. Geophys. Res.*, 116, D14301, <https://doi.org/10.1029/2011JD015643>, 2011.
- Wagner, N. L., Brock, C. A., Angevine, W. M., Beyersdorf, A., Campuzano-Jost, P., Day, D., de Gouw, J. A., Diskin, G. S., Gordon, T. D., Graus, M. G., Holloway, J. S., Huey, G., Jimenez, J. L., Lack, D. A., Liao, J., Liu, X., Markovic, M. Z., Middlebrook, A. M., Mikoviny, T., Peischl, J., Perring, A. E., Richardson, M. S., Ryerson, T. B., Schwarz, J. P., Warneke, C., Welti, A., Wisthaler, A., Ziemba, L. D., and Murphy, D. M.: In situ vertical profiles of aerosol extinction, mass, and composition over the southeast United States during SENEX and SEAC4RS: observations of a modest aerosol enhancement aloft, *Atmos. Chem. Phys.*, 15, 7085–7102, <https://doi.org/10.5194/acp-15-7085-2015>, 2015.
- Wang, H.: Formation of nascent soot and other condensed-phase materials in flames, *P. Combust. Inst.*, 33, 41–67, <https://doi.org/10.1016/j.proci.2010.09.009>, 2011.
- Warneke, C., de Gouw, J. A., Edwards, P. M., Holloway, J. S., Gilman, J. B., Kuster, W. C., Graus, M., Atlas, E., Blake, D., Gentner, D. R., Goldstein, A. H., Harley, R. A., Alvarez, S., Rappenglueck, B., Trainer, M., and Parrish, D. D.: Photochemical aging of volatile organic compounds in the Los Angeles basin: Weekday-weekend effect, *J. Geophys. Res.-Atmos.*, 118, 5018–5028, <https://doi.org/10.1002/jgrd.50423>, 2013.
- Weinheimer, A. J., Walega, J. G., Ridley, B. A., Gary, B. L., Blake, D. R., Blake, N. J., Rowland, F. S., Sachse, G. W., Anderson, B. E., and Collins, J. E.: Meridional distributions of  $\text{NO}_x$ ,  $\text{NO}_y$ , and other species in the lower stratosphere and upper troposphere during AASE II, *Geophys. Res. Lett.*, 21, 2583–2586, 1994.
- Wilkinson, G. H. and Rogers, C. E.: Symbolic Description of Factorial Models for Analysis of Variance, *Appl. Stat.*, 22, 392–399, 1973.
- Wilson, E. B.: First and second laws of error, *J. Am. Stat. Assoc.*, 18, 841–851, 1923.
- Wisthaler, A., Crawford, J. H., Haidacher, S., Hanel, G., Hartungen, E., Jordan, A., Märk, L., Mikoviny, T., Müller, M., Mutschlechner, P., Schottkowsky, R., Sulzer, P., Crawford, J. H., and Wisthaler, A.: Development of a compact PTR-ToF-MS for suborbital research on the earth's atmospheric composition, in: 6th International Conference on Proton Transfer Reaction Mass

- Spectrometry and its Applications, 27 April–2 May 2014, Vienna, Austria, Contributions, Innsbruck University Press, 96–96, 2014.
- Yates, E. L., Schiro, K., Lowenstein, M., Sheffner, E. J., Iraci, L. T., Tadić, J. M., and Kuze, A.: Carbon Dioxide and Methane at a Desert Site – A Case Study at Railroad Valley Playa, Nevada, USA, *Atmosphere*, 2, 702–714, 2011.
- Yokelson, R. J., Griffith, D. W. T., and Ward, D. E.: Open-path Fourier transform infrared studies of large-scale laboratory biomass fires, *J. Geophys. Res.*, 101, 21067–21080, <https://doi.org/10.1029/96JD01800>, 1996.
- Yokelson, R. J., Karl, T., Artaxo, P., Blake, D. R., Christian, T. J., Griffith, D. W. T., Guenther, A., and Hao, W. M.: The Tropical Forest and Fire Emissions Experiment: overview and airborne fire emission factor measurements, *Atmos. Chem. Phys.*, 7, 5175–5196, <https://doi.org/10.5194/acp-7-5175-2007>, 2007.
- Yokelson, R. J., Andreae, M. O., and Akagi, S. K.: Pitfalls with the use of enhancement ratios or normalized excess mixing ratios measured in plumes to characterize pollution sources and aging, *Atmos. Meas. Tech.*, 6, 2155–2158, <https://doi.org/10.5194/amt-6-2155-2013>, 2013.